Fermi liquid approach to the quantum *RC* circuit: Renormalization group analysis of the Anderson and Coulomb blockade models

Michele Filippone and Christophe Mora

Laboratoire Pierre Aigrain, École Normale Supérieure, Université Paris 7 Diderot, CNRS; 24 rue Lhomond, 75005 Paris, France

(Received 10 May 2012; revised manuscript received 19 July 2012; published 12 September 2012)

We formulate a general approach for studying the low-frequency response of an interacting quantum dot connected to leads in the presence of oscillating gate voltages. The energy dissipated is characterized by the charge relaxation resistance, which under the loose assumption of Fermi liquid behavior at low energy, is shown to depend only on static charge susceptibilities. The predictions of the scattering theory are recovered in the noninteracting limit while the effect of interactions is simply to replace densities of states by charge susceptibilities in formulas. In order to substantiate the Fermi liquid picture in the case of a quantum *RC* geometry, we apply a renormalization group analysis and derive the low-energy Hamiltonian for two specific models: the Anderson and the Coulomb blockade models. The Anderson model is shown, using a field theoretical approach based on Barnes slave bosons, to map onto the Kondo model. We recover the well-known expression of the Kondo temperature for the asymmetric Anderson model and compute the charge susceptibility. The Barnes slave bosons are extended to the Coulomb blockade model where the renormalization-group analysis can be carried out perturbatively up to zero energy. All calculations agree with the Fermi liquid nature of the low-energy fixed point and satisfy the Friedel sum rule.

DOI: 10.1103/PhysRevB.86.125311 PACS number(s): 71.10.Ay, 73.63.Kv, 72.15.Qm

I. INTRODUCTION

The ability to probe and manipulate electrons in real time constitutes one of the main challenges of transport in quantum dots. This program is spurred by technological progress in guiding and processing high-frequency electronic signals. At low frequency, charge or spin can be transferred adiabatically with quantum pumps[1–6] and single-electron tunneling events can be measured by coupling the system to a nearby quantum point contact,[7,8] the detection bandwidth is, however, restricted to the kilohertz regime. These low-frequency experiments may control and monitor single-charge transfer events but they are not able to capture the coherent dynamics of charge carriers.

Early experiments at high frequency used a microwave source (typically above the gigahertz) to irradiate the quantum dot in the presence of a source-drain dc bias voltage.[9,10] The energy of a photon $\hbar\omega$ may exceed the thermal energy k_BT and photon-assisted tunneling takes place. Electrons are then able to tunnel across the quantum dot by emitting or absorbing photons from the microwave signal. Probing quantum dots at high frequency provides information on the quantum motion of electrons.[11] The microwave part of the noise power spectrum corresponds to the typical energies (level spacing, charging energy, etc.) of quantum dots of micrometer size. In the quantum regime $\hbar\omega > k_BT$, the noise emitted by a nanoconductor device can be absorbed and measured by an on-chip quantum detector. Different schemes have been developed where the quantum detector, located in the vicinity of the source, can be a quantum dot,[12–14] a SIS tunnel junction,[15–17] or a superconducting resonator.[18] An alternative way to measure directly the emitted noise from the nanoconductor is to use cryogenic low-noise amplifiers.[19–21] This nonexhaustive synopsis of high-frequency experiments demonstrates the vitality of research in this field.

A fundamental and paradigmatic experiment[22] in the topic of high-frequency transport is the quantum capacitor, or quantum *RC* circuit. It consists of a quantum dot attached to a reservoir lead via a quantum point contact. In the experiment of Refs. 22–24, a single spin-polarized channel of the lead is connected to the quantum dot. In addition, the quantum dot forms a mesoscopic capacitor with a top metallic gate as illustrated in Fig. 1. These resistive and capacitive elements constitute the quantum analog of the classical *RC* circuit in series. By applying a time-dependent voltage on the top gate, the quantum capacitor can be operated in the linear[22] or nonlinear[23–25] regime, and charge can be transferred between the dot and the lead alternatively. In the linear regime, an ac drive changes infinitesimally and periodically the charge of the dot. Matching the low-frequency admittance of the dot with the corresponding formula for a classical *RC* circuit,

$$\frac{I(\omega)}{V_g(\omega)} = -i\omega C_0(1 + i\omega C_0\, R_q) + O(\omega^3), \qquad (1)$$

allows us to define a quantum capacitance C_0 and a charge relaxation resistance R_q. V_g denotes the gate voltage and I is the current from the dot to the lead.

Recent experiments have developed an alternative way of measuring the admittance of a single or double quantum dot by embedding it in a microwave cavity,[26,27] see also experiments using radiofrequency reflectometry.[28–30] A good quality factor greatly enhances the coupling to the photons at the resonant frequencies of the cavity and the admittance can be read off the phase of a microwave probe. Only measurements of the capacitance[31] were realized so far but the technique is, in principle, able to capture the charge relaxation resistance.

The term *charge relaxation resistance* was coined in the seminal work of Büttiker, Prêtre, and Thomas[32–34] where a general theory of time-dependent coherent transport was put forward. Coulomb interactions were treated using a discrete RPA-like model in which the screening of the potential imposed by the gate is taken into account self-consistently. One particular outcome of this theory is the prediction of a

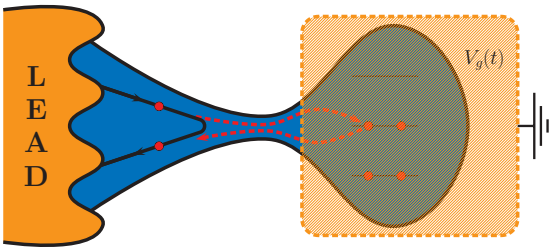

FIG. 1. (Color online) Schematic view of the quantum RC circuit. Electrons coming from a metallic lead can tunnel inside a quantum dot where there are interactions between electrons. An oscillating voltage $V_g(t)$ is applied by a metallic gate coupled capacitively to the dot.

quantized and universal resistance $R_q = h/2e^2$ in the case of a polarized single-channel lead. This remarkable universality was notably confirmed experimentally.[22] For more than one channel, R_q was expressed in terms of statistical distribution of dwell times, corresponding in that case to Wigner-Smith delay times,[35,36] and computed for chaotic or weakly disordered quantum dots using random matrix theory techniques.[37–40] Interestingly, the RPA-like screening approximation emerges as the leading order contribution in an $1/N$ expansion (N being the number of channels in the lead connected to the dot). This expansion was devised[41] as a general method to describe the interplay of coherent transport and interaction in quantum dots driven out of equilibrium. Other aspects of the linear ac response of the quantum RC circuit were theoretically addressed including the charge relaxation resistance and the inductive response[42] within a Luttinger model for a long tube connected between electrodes,[43,44] the quantum to classical transition in the presence of finite temperature or dephasing probes[45,46] and the effect of possibly strong interaction within an Hartree-Fock approach[47–49] or by developing a real-time diagrammatic expansion in the tunnel coupling.[50] It has also been suggested that the quantum RC circuit could be used to detect efficiently the state of a nearby double-dot system[51] or to probe charge fractionalization in a quantum spin-Hall insulator.[52]

The charge relaxation resistance has also been investigated for small metallic islands where the tunnel junction to the reservoir is described by a large number of weakly transmitting channels.[53,54] In this regime, a mapping to the problem of a single particle on a ring subject to dissipation has been exploited[55] to demonstrate a new fixed point at large transparency associated to the quantized resistance $R_q = h/e^2$.

Before pursuing our discussion on the linear ac response, let us mention that the experiment[22] on the quantum RC circuit was also driven into a nonlinear regime.[23–25] A square-shaped excitation with an amplitude comparable to the level spacing turns the mesoscopic capacitor into a single electron source. An electron (and a hole) is thus sent into the lead at each period of the driving signal. This experiment has initiated an intense theoretical activity on dynamics and quenches in coherent and interacting nanoscaled systems.[56–62]

The prediction of the universal resistance $R_q = h/2e^2$ for a single channel was recently reconsidered[63,64] by treating Coulomb interaction in an exact manner. In this way, the strong Coulomb blockade regime could be addressed analytically, yet at the price of treating the coupling to the lead perturbatively, for either small or large transparency. All analytical calculations: bosonization of the fermionic degrees of freedom, perturbation in the dot-lead coupling and mapping to the Kondo model,[65,66] point to the fact that the resistance $R_q = h/2e^2$ survives arbitrarily strong interactions for all transmissions, thereby reinforcing its universality. In addition to this result, it was shown[63] that a large dot, with an effectively vanishing level spacing, also supports a universal, albeit different, charge relaxation resistance $R_q = h/e^2$. Interactions in the lead, for the edge state of a fractional quantum Hall state for instance, are added[63,64] for free in bosonization. They simply renormalize the charge relaxation resistance $R_q = h/2\nu e^2$, where ν denotes the electron filling factor in the bulk. For $\nu < 1/2$, a quantum phase transition occurs[64] as a function of the transmission (dot-lead coupling) into an incoherent regime where resistance quantization is lost (see also Ref. 67 where a similar transition was obtained). Complementary to these analytical findings, Monte Carlo calculations[64] have confirmed the universality of the charge relaxation resistance for $\nu > 1/2$ (including the case of noninteracting leads $\nu = 1$), i.e., for all interactions and transmissions and the quantum phase transition for $\nu < 1/2$.

Surprises came from the single-channel case with spinfull electrons (in contrast to the fully polarized edge states). When a single level on the dot participates to electronic transport, the quantum RC circuit is described by the Anderson model.[68] At zero magnetic field and small excitation frequency, the Korringa-Shiba relation[69] on the dynamical charge susceptibility implies a quantized universal resistance $R_q = h/4e^2$, again in agreement with the original RPA approach.[47] Note that this corresponds to a weak charge response and a weak low-frequency dissipation $\propto C_0^2 R_q$ when the charge on the dot is quenched by strong Coulomb interaction (for example, in the Kondo regime). Finite magnetic fields or higher frequencies do not alter the freezing of charge fluctuations, but they allow processes that redistribute the spin populations on the dot and cause an increase of energy dissipation. The result is a giant peak that the charge relaxation resistance develops with either frequency or magnetic field.[70] Note that although the peak in magnetic field emerges at the Kondo energy scale and therefore originates from strong correlations, it does not contradict the Fermi liquid nature of the model at low frequency but arbitrary magnetic field. A Fermi liquid description[71] is thus able to reproduce analytically the properties of the peak, showing that the peak disappears at the particle-hole symmetric point. A generalized Korringa-Shiba relation can be derived that expresses the resistance R_q in terms of static susceptibilities. As we shall discuss in this paper, the Fermi liquid approach introduced in Refs. 71 and 72 is, in fact, quite general and should apply to a variety of models.

To summarize, analytical and numerical calculations[63,64] have proven that the universal resistance $R_q = h/2e^2$ remains valid even for strong Coulomb interaction on the dot. Nevertheless, the physical reason for this universality is somehow hidden in the formalism, especially in the bosonization approach. The intent of this paper is to bridge the gap between the weakly interacting model of Refs. 32–34 and 49 and the strongly interacting approach of Refs. 63 and 64, by proposing a general Fermi liquid framework that captures all interaction

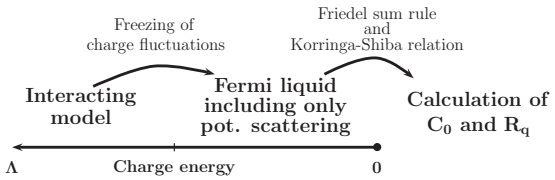

FIG. 2. Line of reasoning developed in this paper. The linear response of interacting systems is described by a noninteracting Fermi liquid at low energy. It is then possible to compute the quantum capacitance C_0 and the charge relaxation resistance R_q. Λ is the cutoff energy scale in the RG approach.

regimes within a single model, and recovers $R_q = h/2e^2$ in the single-channel case.

The paper is organized essentially along two directions. The first part, corresponding to Sec. II, presents the main ideas underlying the Fermi liquid approach. Due to the lack of phase-space available for inelastic scattering (this is the standard Landau argument for Fermi liquids[73–75]), elastic processes dominate the physics of interacting quantum dots at low energy.[76] Hence low energies are described by noninteracting electrons backscattered by the dot and, using the Friedel sum rule,[77] one arrives at the Korringa-Shiba formula for the dynamical charge susceptibility. While the capacitance is proportional to the local charge susceptibility, $C_0 = e^2\chi_c$, the charge relaxation resistance is expressed as a combination of static charge susceptibilities given by Eq. (24), with $R_q = h/2e^2$ in the single-channel case. The discussion is extended to the case of a large dot in Sec. II E, where the dot itself is described as a Fermi liquid of noninteracting electrons separated from the lead, and the charge relaxation resistance is in units of $R_q = h/e^2$. Both resistances, $h/2e^2$ and h/e^2, are direct consequences of the Fermi liquid structure (14) and of the Friedel sum rule, and are therefore almost independent of the gate voltage.

The second part of the paper is detailed in Sec. III. The validity of the Fermi liquid approach is explored using a renormalization group (RG) analysis for two specific models relevant to describe the quantum *RC* circuit: the Anderson and the Coulomb blockade models. This is illustrated in Fig. 2. The perturbative RG approach allows us, for both models, to calculate explicitly the low-energy effective Hamiltonian in agreement with Sec. II. In particular, the Friedel sum rule is checked by comparing our predictions with existing results from the literature: Bethe-ansatz calculations for the Anderson model and a perturbative calculation for the Coulomb blockade model. In addition for the Anderson model, we provide a rigorous mapping to the Kondo model and derive an analytic formula for the charge susceptibility in powers of the hybridization out of the particle-hole symmetric point.

II. FERMI LIQUID APPROACH

A. Hamiltonians

The Fermi liquid approach, to be discussed below in the core of this section, does not rely on a specific Hamiltonian but rather defines a universality class for the low-energy behavior of coupled dot and lead systems. Despite of this, we will introduce two particular Hamiltonians: the Anderson model[68] and a second model describing an interacting quantum dot with internal levels that we shall call the Coulomb blockade model (CBM).[65,66] For these two models indeed, we shall see in Sec. III that they fall into the category of Fermi liquids at low energy. Nevertheless, one has to keep in mind that the conclusions of this section are in no way restricted to the models Eqs. (2) and (3) but would also be applicable for more complicated interactions on the dot mixing, for example, long-range and short-range components.

The quantum *RC* circuit is described[70,71] by the Anderson model when the level spacing in the dot is sufficiently large and electron transport is not spin polarized. The Hamiltonian takes the form

$$H_{\rm AM} = \sum_{\sigma,k} \varepsilon_{k\sigma} c^\dagger_{k\sigma} c_{k\sigma} + \varepsilon_d\, \hat{n} + U \hat{n}_\uparrow \hat{n}_\downarrow + t \sum_{k,\sigma} (c^\dagger_{k\sigma} d_\sigma + d^\dagger_\sigma c_{k\sigma}), \tag{2}$$

with the electron operators $c_{k\sigma}$ and d_σ of spin σ for the lead and the dot, respectively. The lead electrons are characterized by the single-particle energies ε_k with the constant density of states ν_0. The electron number on the dot is $\hat{n} = \hat{n}_\uparrow + \hat{n}_\downarrow$ with $\hat{n}_\sigma = d^\dagger_\sigma d_\sigma$. U is the interaction energy, or the charging energy in the case of a quantum dot, related to the gate capacitance C_g through $U = e^2/C_g$. $\varepsilon_d = -eV_g$ is the single-level energy of the dot. It is tuned via the electrostatic coupling of the quantum dot to the metallic gate. t is the amplitude for electron tunneling between the dot and the lead. We will later need the hybridization constant $\Gamma = \pi \nu_0 t^2$.

The second model, which we call the Coulomb blockade model (CBM),[65,66] is appropriate for a larger dot with at least a few energy levels in the dot relevant for transport. Its simplest version includes spinless electrons and a single channel in the lead but it can be straightforwardly extended to N channels. The Hamiltonian splits as[63,78] $H_{\rm CBM} = H_0 + H_c + H_T$ with

$$H_0 = \sum_{k,\sigma} \varepsilon_k\, c^\dagger_{k\sigma} c_{k\sigma} + \sum_{l,\sigma} \varepsilon_l\, d^\dagger_{l\sigma} d_{l\sigma} + \varepsilon_d\, \hat{n}, \tag{3a}$$

$$H_c = E_c \hat{n}^2, \quad H_T = t \sum_{k,l,\sigma} (d^\dagger_{l\sigma} c_{k\sigma} + c^\dagger_{k\sigma} d_{l\sigma}), \tag{3b}$$

where the three terms describe, respectively, noninteracting electrons with single-particle energies ε_k (lead) and ε_l (dot), the charging energy due to strong Coulomb repulsion in the dot and the tunneling of electrons between the dot and the lead. $E_c = e^2/2C_g$ and $\sigma = 1, \ldots, N$. Again, $\hat{n} = \sum_\sigma \hat{n}_\sigma = \sum_{k,\sigma} d^\dagger_{k\sigma} d_{k\sigma}$ is the total number of electrons in the dot and $\varepsilon_d = -eV_g$ is set by the gate voltage. The level spacing in the dot is finite but can be sent to zero for a large enough quantum dot. In this paper, the density of states ν_0 is chosen for simplicity to be the same in the lead and in the dot but none of our results are affected by releasing this constraint. It will be convenient later to use the dimensionless conductance $g = N\,(\nu_0\, t)^2$. For both models, the total number of electrons, that is a constant of motion, is written $\hat{N}_t$.

Although the derivations of Sec. III are valid only away from charge degeneracy, the Anderson and the one-channel Coulomb blockade models are both Fermi liquids for all gate voltages ε_d. Our effective Fermi liquid approach, which

predicts the resistances $h/2e^2$ and h/e^2, is therefore applicable for all values of ε_d including the Coulomb peaks at the charge degeneracy points. In the multichannel Coulomb blockade model, the Fermi liquid approach breaks down only right at charge degeneracy (non-Fermi liquid fixed points).

B. Noninteracting electrons

Before addressing the general Fermi liquid approach, which is the central part of this paper, it is instructive to shortly review the noninteracting case[32–34] following the discussion of Ref. 49. First, the coupling to the gate voltage $\varepsilon_d(t)\hat{n}$ can be gauged out by a simple unitary transformation $U(t) = e^{i\int^t dt' \varepsilon_d(t')\hat{N}_t}$ shifting all single-particle energies by $-\varepsilon_d$, notably, $\varepsilon_k \to \varepsilon_k - \varepsilon_d$ for the single-particle energies in the lead.

Coherent electrons are described by delocalized wave functions propagating throughout the quantum dot. Different trajectories, corresponding to single or multiple reflections at the quantum point contact opening the dot, interfere by adding their amplitudes. In the absence of Coulomb interaction, electrons behave very much like photons traversing a dispersive medium: an energy-dependent phase shift $\Phi(\varepsilon_k - \varepsilon_d)$ is accumulated after passing through the dot. Although the discussion here is meant to be general, we can illustrate with a specific example. The phase shift reads

$$e^{i\Phi(\varepsilon)} = \frac{r - e^{i2\pi\varepsilon/\Delta}}{1 - re^{i2\pi\varepsilon/\Delta}} \tag{4}$$

for a quantum dot embedded in a quantum Hall edge state, r being the reflection coefficient of the quantum point contact, Δ the level spacing in the dot and $2\pi\varepsilon/\Delta$ the phase accumulated after a single turn around the dot. With this picture in mind, the current from the dot to the lead can be computed from the Landauer-Büttiker scattering formalism.[32–34,49] At low frequency,

$$I(t) = \frac{e^2}{h}[V_g(t) - V_g(t-\tau)], \tag{5}$$

τ is the Wigner-Smith delay time, or the typical dwell time of an electron in the dot (ε_F is the Fermi energy),

$$\tau = \hbar \left.\frac{d\Phi(\varepsilon - \varepsilon_d)}{d\varepsilon}\right|_{\varepsilon=\varepsilon_F} = -\hbar\frac{d\Phi(\varepsilon_F - \varepsilon_d)}{d\varepsilon_d}, \tag{6}$$

and Eq. (5) holds as long as $\omega\tau \ll 1$.

Equation (5) and (6) show that a nonzero current is an effect of the dispersive cavity. Physically, a time varying gate voltage $\varepsilon_d(t)$ implies that different times of electron arrivals correspond to different energies $\varepsilon - \varepsilon_d(t)$ and therefore different phase shifts. All electrons are not slowed down in the same way and charge can accumulate either in the dot or in the lead. Fourier transform of Eq. (5) is compared to Eq. (1) and yields

$$R_q = \frac{h}{2e^2}, \tag{7a}$$

$$C_0 = \frac{e^2}{h}\tau, \tag{7b}$$

such that $\tau = 2R_qC_0$. The coherent regime thus gives a quantized and universal resistance $R_q = h/2e^2$.

The same reasoning applies to the case of N channels in the lead connected to the dot. The result for the charge relaxation resistance reads[39,47]

$$R_q = \frac{h}{2e^2}\frac{\sum_{\sigma=1}^N \tau_\sigma^2}{\left(\sum_{\sigma=1}^N \tau_\sigma\right)^2} = \frac{h}{2e^2}\frac{\sum_{\sigma=1}^N \nu_{0\sigma}^2}{\left(\sum_{\sigma=1}^N \nu_{0\sigma}\right)^2}, \tag{8}$$

where τ_σ is the Wigner-Smith delay time in the channel σ. $\nu_{0\sigma} = \tau_\sigma/h$[39] denotes the density of states for channel σ in the dot.

C. Physical picture

Simple arguments can be given to argue that the results Eq. (7) extend to the general case of interacting electrons. Despite its apparent simplicity, the expression Eq. (6) for the time delay τ that controls the low-frequency transport, conveys a fundamental message: only electrons in the immediate vicinity of the Fermi surface participate to ac transport at low frequency. These electrons, however, following the conventional Fermi liquid argument,[73–75] are somehow protected against interactions due to the restriction of available phase-space close to the Fermi surface. Hence, even in the presence of strong Coulomb repulsion on the dot, low-energy electrons in the lead behave essentially as if they were noninteracting and the line of reasoning detailed above generalizes to the interacting case. This generalization is possible only in the generic situation of Fermi liquid behavior at low energy while non-Fermi liquid fixed points usually require a delicate tuning of coupling constants.[79–81] We note in passing that a similar restoration of phase-coherence caused by Coulomb interaction was explored in a quantum dot T-junction geometry.[76]

Relatedly, Eq. (7b) for the capacitance or the static response of the dot, coincides with an exact expression as we shall now argue. In the interacting case, the phase shift $\delta(\varepsilon_d) = \Phi(\varepsilon_k - \varepsilon_d)/2$ (there is factor 2 difference between the phase shift definition used in the noninteracting case for instance in Refs. 22 and 49, and the conventional phase shift of the Friedel sum rule[77]) is related to the occupancy of the dot via the Friedel sum rule $\delta/\pi = \langle\hat{n}\rangle$. Substituted in Eq. (7b), one finds

$$C_0 = -2\pi\frac{\partial\langle\hat{n}\rangle}{\partial\varepsilon_d}\frac{e^2}{2\pi} = e^2\chi_c, \tag{9}$$

where χ_c is the static charge susceptibility of the dot. This result coincides with the mere definition of C_0 if we recall that $I = \partial_t\, e\langle\hat{n}\rangle$ and consider the time-integrated version of Eq. (1) in the static limit.

Let us now clarify an important point: the similarities between the scattering properties of noninteracting and interacting electrons do not imply that interactions have no effect as they can strongly renormalize the energy dependence of the phase shift. For noninteracting electrons, a comparison between Eqs. (7b) and (9) suggests that $\tau/h = \nu_{d0} = \chi_c$, clearly a sensible result. Indeed, for free electrons, the density of states represents the number of one-particle states that fall below the Fermi surface upon a unit increase of the Fermi energy or, equivalently, a unit decrease of the reference energy ε_d. The Pauli principle then implies that it is also the number of added electrons, that is the charge susceptibility. However, in the presence of interactions between electrons, $\nu_{d0} \neq \chi_c$, in general. χ_c is sensitive only to charge excitations while

all excitations contribute to the density of states ν_{d0}. This difference is exemplified[70,71] by the Anderson model in the Kondo regime where the local density of states exhibits a peak at the Fermi energy, mostly due to spin-flip excitations, whereas the charge susceptibility is suppressed by Coulomb blockade.[82]

D. Effective model and Korringa-Shiba formulas

We begin by some general remarks on dissipation for the quantum RC circuit. Integrating Eq. (1) with respect to time, we find the low-frequency expansion[63,71]

$$\frac{e^2\langle\hat{n}(\omega)\rangle}{-\varepsilon_d(\omega)} = C_0 + i\omega C_0^2 R_q + \mathcal{O}(\omega^2), \tag{10}$$

for the charge on the dot in the presence of a time-dependent gate voltage. The comparison with standard linear response theory allows for deriving the correspondences

$$\chi_c(\omega=0) = \frac{C_0}{e^2}, \quad \mathrm{Im}\,\chi_c(\omega)|_{\omega\to 0} = \frac{\omega C_0^2 R_q}{e^2}, \tag{11}$$

with the dynamical charge susceptibility

$$\chi_c(t-t') = \frac{i}{\hbar}\theta(t-t')\langle[\hat{n}(t),\hat{n}(t')]\rangle. \tag{12}$$

Following standard linear response theory, the power dissipated in the presence of an ac drive of the gate voltage, $\varepsilon_d(t) = \varepsilon_d^0 + \varepsilon_\omega \cos\omega t$ with ε_ω small enough to be in the linear regime, is given quite generally, and specifically in the models Eqs. (2) and (3), by

$$\mathcal{P} = \tfrac{1}{2}\varepsilon_\omega^2\,\omega\,\mathrm{Im}\chi_c(\omega). \tag{13}$$

The only requirement for Eq. (13) to hold is that ε_d appears in the Hamiltonian only through the term $\varepsilon_d\,\hat{n}$.

Having exposed in Sec. II C the physical reasons for which the universal resistance is insensitive to arbitrary interaction in the dot, we proceed and develop a low-energy effective model that shall prove Eq. (7a) explicitly. General arguments are sufficient to reconstruct the structure of the low-energy effective Hamiltonian. Nevertheless, one has to keep in mind that the whole discussion that follows is based on the assumption of a Fermi liquid infrared (IR) fixed point.

The first piece of the Hamiltonian is a free part $H_0 = \sum_k \varepsilon_k c_k^\dagger c_k$. It describes the bulk lead electrons. The dot having a finite spatial extension, it is not able to alter the bulk properties (like the Fermi velocity or the effective mass) of the lead electrons. Operators perturbing the free term H_0 can be classified, in the RG sense, according to their relevance. Again the finite size of the dot implies that these operators involve only the field operators $\psi(\mathbf{r}=0) = \sum_k c_k$, $\mathbf{r}=0$ being the entrance of the dot or the position of the quantum point contact, $\psi^\dagger(0)$ and derivatives thereof. There is only a single marginal operator, all other operators being irrelevant. Keeping the former and discarding the latter, the low-energy Hamiltonian assumes the form

$$H = \sum_k \varepsilon_k c_k^\dagger c_k + K(\varepsilon_d)\sum_{k,k'} c_k^\dagger c_{k'}. \tag{14}$$

The second term in this Hamiltonian describes a structureless scattering potential [$\propto\delta(\mathbf{r})$] placed at the dot-lead boundary or entrance of the dot. For the two initial models Eqs. (2) and (3), the Friedel sum rule relates the phase shift of this scattering potential to the mean occupation of the dot,[77] namely,

$$\langle\hat{n}\rangle = -\frac{1}{\pi}\arctan[\pi\nu_0 K(\varepsilon_d)]. \tag{15}$$

Drawing on the ideas of Refs. 71 and 72, the strategy that we shall adopt to compute the charge relaxation resistance is the following: the power dissipated by the gate voltage $\varepsilon_d(t) = \varepsilon_d^0 + \varepsilon_\omega\cos\omega t$ in the linear regime, given by Eq. (13), can also be computed from the low-energy model Eq. (14). The identification between the general expression Eq. (13) and the low-energy calculation allows us to derive a Korringa-Shiba formula for $\mathrm{Im}\chi_c(\omega)$, which further determines R_q.

Let us now start from the low-energy Hamiltonian and expand it to first order with respect to ε_ω [$K_0 = K(\varepsilon_d^0)$],

$$H = \sum_k \varepsilon_k c_k^\dagger c_k + K_0\sum_{k,k'} c_k^\dagger c_{k'} + K'(\varepsilon_d^0)\,\varepsilon_\omega\cos\omega t\sum_{k,k'} c_k^\dagger c_{k'}. \tag{16}$$

The scattering by the potential $K_0\delta(\mathbf{r})$ is a single-particle problem, which can be readily diagonalized. Rewriting the Hamiltonian in terms of the corresponding scattering states, characterized by the fermionic operators $\tilde{c}_k$, absorbs the second term into the first one in Eq. (16). Additionally, this change of basis introduces a multiplicative constant[83] in the third term of Eq. (16) and

$$H = \sum_k \varepsilon_k \tilde{c}_k^\dagger\tilde{c}_k + \frac{K'(\varepsilon_d^0)\,\varepsilon_\omega\cos\omega t}{1+(\pi\nu_0 K_0)^2}\sum_{k,k'}\tilde{c}_k^\dagger\tilde{c}_{k'}. \tag{17}$$

This last expression is conveniently written in terms of the static susceptibility $\chi_c = -\partial\langle\hat{n}\rangle/\partial\varepsilon_d$, which is obtained through the derivative of Eq. (15):

$$\chi_c = \frac{\nu_0\,K'(\varepsilon_d^0)}{1+(\pi\nu_0 K_0)^2}, \tag{18}$$

such that Eq. (17) becomes

$$H = \sum_k \varepsilon_k \tilde{c}_k^\dagger\tilde{c}_k + \frac{\chi_c}{\nu_0}\varepsilon_\omega\cos\omega t\sum_{k,k'}\tilde{c}_k^\dagger\tilde{c}_{k'}. \tag{19}$$

It can be checked for consistency that this low-energy model satisfies the Friedel sum rule in the static limit $\omega\to 0$. The scattering potential in Eq. (19) adds the phase shift $\delta_1 = -\pi\nu_0\frac{\chi_c}{\nu_0}\varepsilon_\omega$ to lead electron wave functions. The Friedel sum rule then translates this phase shift into a shift in the occupation number on the dot:

$$\delta\langle\hat{n}\rangle = \delta_1/\pi = -\chi_c\,\varepsilon_\omega, \tag{20}$$

in agreement with the above definition of the static charge susceptibility.

Now that we have derived a more compact low-energy Hamiltonian, we rely again on linear response theory in order to compute the power dissipated upon exciting the gate voltage sinusoidally. It involves the operators $\hat{A} = (\chi_c/\nu_0)\sum_{k,k'}\tilde{c}_k^\dagger\tilde{c}_{k'}$ coupled to the ac drive in Eq. (19) or

$$\mathcal{P} = \tfrac{1}{2}\varepsilon_\omega^2\,\omega\,\mathrm{Im}\,\chi_{\hat{A}}(\omega), \tag{21}$$

where $\chi_{\hat{A}\sigma}(t-t') = \frac{i}{\hbar}\theta(t-t')\langle[\hat{A}_\sigma(t), \hat{A}_\sigma(t')]\rangle$. Perhaps unsurprisingly, energy dissipation occurs at low energy through the production of single electron-hole excitation. $\mathrm{Im}\chi_A(\omega)$ is easily computed at zero temperature for noninteracting electrons [first term in Eq. (19)], $\mathrm{Im}\chi_{\hat{A}}(\omega) = \hbar\pi\chi_c^2\omega$, similar to the result of a Fermi golden rule calculation. Comparing Eqs. (13) and (21), we obtain the Korringa-Shiba formula[69]

$$\mathrm{Im}\chi_c(\omega) = \hbar\pi\omega\,\chi_c^2. \tag{22}$$

This result, substituted in Eq. (11), recovers the universal charge relaxation resistance $R_q = h/2e^2$.

So far, our analysis has concentrated on the single channel case but its generalization to N channels is straightforward. One then finds a generalized Korringa-Shiba formula

$$\mathrm{Im}\chi_c(\omega) = \hbar\pi\omega\sum_{\sigma=1}^{N}\chi_{c\sigma}^2. \tag{23}$$

The static susceptibilities $\chi_{c\sigma} = -\partial\langle\hat{n}_\sigma\rangle/\partial\varepsilon_d$ measure the sensitivity of the occupations of the dot, for each channel σ, to a change in the gate voltage. The charge relaxation resistance thus takes the form

$$R_q = \frac{h}{2e^2}\frac{\sum_{\sigma=1}^{N}\chi_{c\sigma}^2}{\left(\sum_{\sigma=1}^{N}\chi_{c\sigma}\right)^2} \tag{24}$$

and resembles very much the noninteracting one Eq. (8). They coincide after the identification $\nu_{0\sigma} = \chi_{c\sigma}$, already discussed in Sec. II C and valid only for free electrons. Therefore Eq. (24) gives the correct generalization of Eq. (8) to the interacting case.

E. Effective model for a large dot

The case of a large quantum dot deserves a specific discussion. By a large dot, we mean that the single-particle spectrum can be treated as continuous in the dot such that energy dissipation takes place both in the lead and in the dot.

In fact, finite dots have a finite level spacing Δ and one may wonder at which energy scale the spectrum can be considered as continuous. One solution, proposed in Ref. 63, is to send an ac signal with a bandwidth larger than Δ in order to smear the discreteness of the spectrum. In that case, the frequency ω has to be larger than Δ. A second possibility is to use a frequency ω larger than the energy $\sqrt{\Delta E_{\mathrm{TH}}}$, where $E_{\mathrm{TH}} > \Delta$ is the Thouless energy, or inverse time of diffusion through the dot. Above this energy, it has been shown[84] that the one-particle density of states loses its discreteness due to electron-electron interactions.

The Fermi liquid picture still applies to the large dot with the subtlety that dot and lead constitute two separate Fermi liquids. At low energy, the transfer of electrons between the dot and the lead is energetically prohibited[74] and electrons are effectively fully backscattered at the boundary between the dot and the lead. The effective model for the lead is the same as above [see Eq. (14)] with the potential scattering strength related to the mean occupation of the dot via Eq. (15).

At first glance, it may seem that the dot simply adds an additional channel for dissipation so that Eq. (24) would apply with $N = 2$. However, as we shall see below, there exists a lead/dot symmetry which reestablishes universality in the charge relaxation resistance. We first note that the fact that the charging energy is ascribed to the dot is physically sensible but mathematically arbitrary. Using the fact that the total number of electrons in the system $\hat{N}_t$ is conserved by the Hamiltonian, one can replace $\hat{n} = \hat{N}_t - \hat{n}_L$, $\hat{n}_L$ being the number of electrons in the lead, and transfer the Coulomb interaction to the lead. Therefore the low-energy model for the dot is the same as for the lead, namely, Eq. (14), but the strength of the scattering potential for dot electrons, noted $K_{\mathrm{dot}}(\varepsilon_d)$, is now given by

$$\hat{N}_t - \langle\hat{n}\rangle = \langle\hat{n}_L\rangle = -\frac{1}{\pi}\arctan[\pi\nu_0 K_{\mathrm{dot}}(\varepsilon_d)]. \tag{25}$$

An alternative formulation of the same physics is that the phase shift accumulated after backscattering at the boundary is $\delta(\varepsilon_d)$ for lead electrons and $\delta_t - \delta(\varepsilon_d)$ for dot electrons, where $\delta_t = \hat{N}_t/\pi$. Following the same steps as in Sec. II D, one finds the effective low-energy Hamiltonian

$$H = \sum_{k,\alpha=L/D}\varepsilon_k\tilde{c}_{k\alpha}^\dagger\tilde{c}_{k\alpha} + \frac{\chi_c}{\nu_0}\varepsilon_\omega\cos\omega t\sum_{k,k'}(\tilde{c}_{kL}^\dagger\tilde{c}_{k'L} - \tilde{c}_{kD}^\dagger\tilde{c}_{k'D}), \tag{26}$$

where L/D stands for lead/dot electrons. The Korringa-Shiba formula is then

$$\mathrm{Im}\chi_c(\omega) = 2\hbar\pi\omega\,\chi_c^2 \tag{27}$$

and the charge relaxation resistance $R_q = h/e^2$. The extension to N channels is straightforward.

III. RENORMALIZATION

A. Outline

The aim of this section is to justify in more detail the low-energy form (14) for the Anderson (2) and CBM (3) models. We recall that the discussion of Sec. II D rests on two fundamental assumptions: (i) an infrared (IR) Fermi liquid fixed point and (ii) the Friedel sum rule (15) applies. The two models will be discussed separately.

The Friedel sum rule and the Fermi liquid properties at low energy are well established for the Anderson model.[77,85] Our motivation is thus a practical one: we calculate the scattering potential $K(\varepsilon_d)$ perturbatively to second order in Γ in the Kondo regime. To this end, a RG treatment is first carried out on the Hamiltonian (2) and stopped at intermediate energies $T_K \ll \Lambda \ll U$, where Λ denotes the running energy scale (or cutoff). The RG approach remains perturbative up to these energies and can be performed explicitly. At this stage, charge excitations have been completely integrated out and the Kondo model is obtained, with exchange and scattering potential terms. Proceeding towards lower energies, the RG procedure becomes nonperturbative across the Kondo temperature T_K and we thus rely on the work of Cragg and Llyod.[86–88] They showed that, whereas the exchange term disappears at low energy, leading simply to a $\pi/2$ scattering phase shift, the scattering potential is unaffected by the Kondo crossover up to small corrections that are negligible within our second-order calculation. The main steps of the RG procedure up to the IR fixed point are summarized in Fig. 3. We finally obtain the

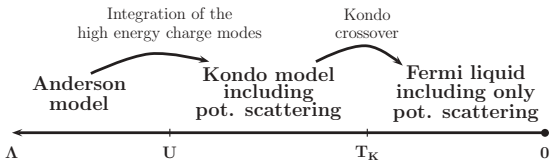

FIG. 3. Renormalization group (RG) analysis of the Anderson model.

scattering potential

$$\nu_0 K(\varepsilon_d) = -\frac{\Gamma}{2\pi}\frac{2\varepsilon_d+U}{\varepsilon_d(\varepsilon_d+U)}\left[1-\frac{\Gamma U}{\pi\varepsilon_d(\varepsilon_d+U)} - \frac{\Gamma U^2}{\pi\varepsilon_d(\varepsilon_d+U)(2\varepsilon_d+U)}\ln\left(\frac{\varepsilon_d+U}{-\varepsilon_d}\right)\right]. \quad (28)$$

This expression can be used to compute the static charge susceptibility χ_c at zero temperature,

$$\chi_c = \frac{\Gamma}{\pi}\left\{\frac{1}{(\varepsilon_d+U)^2}+\frac{1}{\varepsilon_d^2}+\frac{2\Gamma}{\pi}\left[\frac{1}{(\varepsilon_d+U)^3}-\frac{1}{\varepsilon_d^3}\right] + \frac{\Gamma}{\pi}\left[\left(\frac{1}{\varepsilon_d+U}-\frac{1}{\varepsilon_d}\right)^3+2\left(\frac{1}{\varepsilon_d+U}-\frac{1}{\varepsilon_d}\right) \times\left(\frac{1}{\varepsilon_d^2}-\frac{1}{(\varepsilon_d+U)^2}\right)\ln\frac{\varepsilon_d+U}{-\varepsilon_d}\right]\right\}, \quad (29)$$

in agreement with a Bethe ansatz calculation at the particle-hole symmetric point.[89] Let us finally mention that the preliminary perturbative renormalization (stopped at $\Lambda \gg T_K$) recovers Haldane's formula[85,90] for the Kondo temperature of the Anderson model, namely,

$$T_K = \frac{e^{1/4+C}}{2\pi}\sqrt{\frac{2\Gamma U}{\pi}}\, e^{\pi\varepsilon_d(\varepsilon_d+U)/2U\Gamma}, \quad (30)$$

where $C = 0.5772$ is the Euler constant. $e^{1/4+C}/(2\pi) = 0.364$ is in agreement with Ref. 90.

The situation is different for the Coulomb blockade model, which is known to be a Fermi liquid at low energy, except close to the charge degeneracy for $N \neq 1$.[91] For this model, perturbative renormalization can be performed explicitly down to low energy. In this paper, this is done to second order in the conductance g, i.e., to fourth order in the tunneling matrix element t. We are thus able to check the scenario described in Sec. II E of two separated Fermi liquids at low energy with scattering phase shifts in agreement with the Friedel sum rule. To leading order in a large N calculation, we find for the backscattering of lead electrons at the boundary

$$K(\varepsilon_d) = \nu_0 t^2 \ln\frac{E_c+\varepsilon_d}{E_c-\varepsilon_d} + N\nu_0^3 t^4 (A[\varepsilon_d]-A[-\varepsilon_d]), \quad (31)$$

with $A[\varepsilon_d]$ reported in Eq. (90). Translated into the dot occupancy with the help of the Friedel sum rule, this result coincides with a direct calculation by Grabert.[78,92]

Below, we detail the perturbative calculations of the scattering potential $K(\varepsilon_d)$ leading to Eqs. (28) and (31). A refined quantum field theory approach is not necessary for the leading order (first order in Γ) and we simply use the unitary Schrieffer-Wolff transformation to compute $K(\varepsilon_d)$. This is done in Sec. III B. In Secs. III C and III D, the next order is obtained within a more general field theoretical approach to renormalization.

B. Schrieffer-Wolff unitary transformation

When the charging energy, U or E_c, largely exceeds the hybridization to the lead due to tunneling, the different charge states on the dot become well separated in energy. For temperatures $T \ll U, E_c$, one charge state defines the low-energy sector, the others being only virtually occupied. The Schrieffer-Wolff unitary transformation[93] accounts for these virtual states by integrating them perturbatively into an effective Hamiltonian acting in the low-energy sector. The Schrieffer-Wolff transformation was initially devised for the Anderson model, it shall be applied in this paper also to the Coulomb blockade model Eq. (3).

1. Anderson model

We focus on the Kondo regime defined by $0 < -\varepsilon_d < U$, that is in-between the Coulomb peaks, with $|\varepsilon_d|/\Gamma \gg \ln(U/\Gamma)$ in order to neglect the renormalization[85] in the position of these peaks. The low-energy sector then corresponds to a single electron on the dot. The tunneling term in the Anderson model (2), that we call H_T, couples subsequent charge states and is linear in t. The idea of the Schrieffer-Wolff unitary transformation e^{iS} is to cancel this linear tunnel coupling, thereby producing couplings between charge states that have higher orders in t. This strategy is realized with the choice

$$iH_T = \left[S, H^0_{\rm AM}\right], \quad (32)$$

where $H^0_{\rm AM}$ is Eq. (2) with $t = 0$. The rotated Hamiltonian assumes the form

$$H'_{\rm AM} = e^{iS}H_{\rm AM}e^{-iS} = H^0_{\rm AM} + \frac{i}{2}[S, H_T]. \quad (33)$$

After this transformation and specifically for the Anderson model in the Kondo regime, the coupling of the single-charge sector to other charge states starts as t^3 at most. Hence, for the purpose of a calculation up to second order in t, the single-charge sector decouples from other charge states. The resulting effective Hamiltonian is the Kondo model, which includes a potential scattering term:

$$H'_{\rm AM} = H_0 + J\mathbf{S}\cdot\mathbf{s} + K\sum_{kk'\sigma} c^\dagger_{k\sigma}c_{k'\sigma}, \quad (34)$$

where $\mathbf{S}$ denotes the spin operator for the single electron in the dot and $\mathbf{s} = \sum_{kk'\sigma\sigma'} c^\dagger_{k\sigma}\frac{\boldsymbol{\tau}_{\sigma\sigma'}}{2}c_{k'\sigma'}$ the local spin of lead electrons. $\boldsymbol{\tau}_{\sigma\sigma'}$ is the vector composed of the Pauli matrices. The coupling constants are given by

$$\nu_0 J = \nu_0 J_0 = \frac{2\Gamma}{\pi}\left(\frac{1}{\varepsilon_d+U}-\frac{1}{\varepsilon_d}\right), \quad (35a)$$

$$\nu_0 K = \nu_0 K_0 = -\frac{\Gamma}{2\pi}\left(\frac{1}{\varepsilon_d+U}+\frac{1}{\varepsilon_d}\right). \quad (35b)$$

Notice that $K = 0$ at the particle-hole symmetric point $\varepsilon_d = -U/2$, leaving exclusively the Kondo interaction with $J = 8t^2/U$. In deriving the Kondo model Eq. (34), one discards the energy dependence of the coupling constants (35) because the model (34) is applicable only for energies much smaller

than the charging energy $\varepsilon \ll U, |\varepsilon_d|$. The Schrieffer-Wolff transformation is thus an economical way of renormalizing the Anderson model up to the energy scale Λ with $T_K \ll \Lambda \ll U, |\varepsilon_d|$.

Controlling the low-energy behavior, the IR fixed point ($\Lambda \to 0$) of the Kondo model with potential scattering (34), has been identified by Cragg and Llyod using a combination of analytical and numerical calculations.[86–88] It is a Fermi liquid in which lead electrons at the Fermi level acquire a phase shift with three contributions: $\pi/2$, the phase shift corresponding to $K(\varepsilon_d)$ and a correction proportional to Γ^3 that we can legitimately neglect in our first order calculation and even in the second order calculation of Sec. III C. Absorbing the $\pi/2$ phase shift into a redefinition of the lead electrons, we indeed obtain the low-energy form Eq. (14), where $K(\varepsilon_d)$ is given by Eq. (35b).

With the help of the Friedel sum rule (15), the dot occupancy is computed from Eq. (35b) and then the static charge susceptibility at the particle-hole symmetric point reads

$$\chi_c = -\left.\frac{\partial \langle \hat{n} \rangle}{\partial \varepsilon_d}\right|_{\varepsilon_d = -U/2} = \frac{8\Gamma}{\pi U^2}, \tag{36}$$

in agreement with a Bethe ansatz calculation expanded to leading order in Γ/U.[89]

2. *Coulomb blockade model*

In the Coulomb blockade model of Eq. (3), the tunnel coupling between the subsequent charge states is also linear in t and the principle of the Schrieffer-Wolff transformation remains the same as in Sec. III B 1 with the choice Eq. (32) and the rotated Hamiltonian Eq. (33) where the subscript AM is replaced by CBM.

Following Grabert,[78,92] we define the operator $\hat{n}$, which gives the number of electrons in the dot, as being independent from the fermionic degrees of freedom $d_{l\sigma}$ and we note $|n\rangle$ the charge state with n electrons. In this representation, the tunneling term in Eq. (3) reads

$$H_T = t \sum_{n,k,l} (d_l^\dagger c_k |n+1\rangle\langle n| + c_k^\dagger d_l |n-1\rangle\langle n|). \tag{37}$$

For the sake of simplicity, but with no loss of generality, we restrict ourselves here to the single-channel case $N = 1$. The operator S that generates the unitary transformation, solution of Eq. (32), takes the form $s + s^\dagger$ where

$$s = it \sum_{k,l,n} s_{kln} c_k^\dagger d_l |n-1\rangle\langle n|, \tag{38a}$$

$$s_{kln} = \frac{1}{\varepsilon_l - \varepsilon_k + E_C(2n-1) + \varepsilon_d}. \tag{38b}$$

In contrast with the Anderson model, a t^2 coupling between each state $|n\rangle$ with $|n \pm 2\rangle$ is produced by the Schrieffer-Wolff transformation. Nonetheless, it is possible to remove this coupling by applying a second unitary transformation whose specific form will not be needed here. After that, the Hamiltonian becomes block diagonal in the charge states up to second order in t. For $-E_c < \varepsilon_d < E_c$, the charge state $n = 0$ defines the low-energy sector and the rotated Hamiltonian is

$$H'_{\rm CBM} = H_0 + H_{\rm B},$$

$$H_{\rm B} = \frac{t^2}{2} \sum_{kk'll'} (s_{kl0} d_{l'}^\dagger c_{k'} c_k^\dagger d_l - s_{kl1} c_k^\dagger d_l d_{l'}^\dagger c_{k'} + \text{H.c.}). \tag{39}$$

The normal ordering of operators is necessary to classify them according to their RG relevance. For example,

$$d_l^\dagger c_k c_{k'}^\dagger d_{l'} = \delta_{ll'} \theta(-\varepsilon_l) c_k c_{k'}^\dagger + \delta_{kk'} \theta(\varepsilon_k) d_l^\dagger d_{l'} + :d_l^\dagger c_k c_{k'}^\dagger d_{l'}:$$

where $\theta(\varepsilon)$ is the Heaviside function and $:\ldots:$ denotes normal ordering with respect to the Fermi sea. The last term in this expression describes interaction between lead and dot electrons; it is irrelevant at low energy and can be discarded. The two quadratic terms give marginal terms in the Hamiltonian corresponding to backscattering of electrons at the lead-dot boundary. If we take for instance the first one, its contribution to H_B is

$$\begin{aligned} &\frac{t^2}{2} \sum_{kk'} c_{k'} c_k^\dagger \sum_{ll'} \delta_{ll'} \theta(-\varepsilon_l) s_{kl0} \\ &= \sum_{kk'} c_{k'} c_k^\dagger \frac{\nu_0 t^2}{2} \int_{-D_0}^{0} \frac{d\varepsilon_l}{\varepsilon_l - \varepsilon_k - E_c + \varepsilon_d} \\ &= \sum_{kk'} c_k^\dagger c_{k'} \frac{\nu_0 t^2}{2} \ln\left(\frac{\varepsilon_k + E_c - \varepsilon_d + D_0}{\varepsilon_k + E_c - \varepsilon_d}\right). \end{aligned} \tag{40}$$

Since we consider the low-energy properties of the model, it is consistent to take $\varepsilon_k = 0$ in this expression, the difference being again irrelevant in the RG sense. Collecting all marginal terms in Eq. (39) and performing the integrals, we obtain the effective low-energy model to leading order in t:

$$H'_{\rm CBM} = H_0 + \frac{g}{\nu_0} \ln\left(\frac{E_c - \varepsilon_d}{E_c + \varepsilon_d}\right) \left(\sum_{ll'} d_l^\dagger d_{l'} - \sum_{kk'} c_k^\dagger c_{k'}\right), \tag{41}$$

in which the intermediate cutoff D_0 has disappeared[66] and the dimensionless conductance $g = (\nu_0 t)^2$ has been introduced. This expression confirms the scenario proposed in Sec. II E for a large dot in which the two Fermi liquids, lead and dot, completely separate at low energy, while they experience potential scattering terms with opposite amplitudes.

The phase-shift acquired by lead electrons from Eq. (41) is

$$\delta = \pi g \ln\left(\frac{E_c - \varepsilon_d}{E_c + \varepsilon_d}\right) \tag{42}$$

and, applying the Friedel sum rule, one finds the dot mean occupancy

$$\langle \hat{n} \rangle = \frac{\delta}{\pi} = g \ln\left(\frac{E_c - \varepsilon_d}{E_c + \varepsilon_d}\right), \tag{43}$$

in agreement with previous direct perturbative computations[66,78,92] to order g. The above result Eq. (43) is unchanged for N channels as long as $g = N(\nu_0 t)^2$.

As we shall show below, the different conclusions obtained in this section carry over to the next order in g. We were not able to iterate the Schrieffer-Wolff transformation to next orders. We shall instead use a field theoretical approach to derive the renormalization of the two models to second order

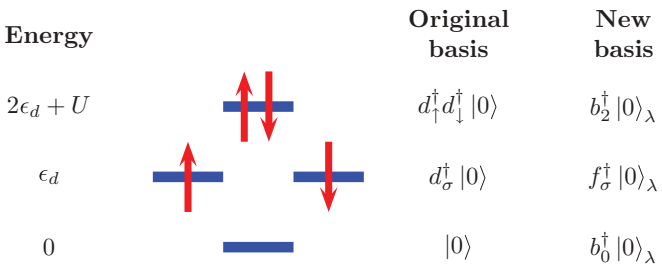

FIG. 4. (Color online) New definition of the states on the dot in Barnes' representation. The energies are given for an isolated dot.

in Γ and g, the Anderson model in Sec. III C and the CBM in Sec. III D.

C. Field theory approach I: Renormalization of the Anderson model

Quantum field theory is an efficient tool for carrying out RG calculations and extracting the low-energy behavior. Standard diagrammatic perturbation techniques are not applicable to the Anderson model when expanded in the tunneling constant t, because of the nonquadratic interaction term $U\hat{n}_\uparrow\hat{n}_\downarrow$. To circumvent this problem, we follow a representation due to Barnes[94] and introduce two slave-boson operators b_0 and b_2, corresponding to the states of the dot with zero and two electrons, respectively. This also necessitates to define two parafermions operators f_σ destroying electrons on the dot. The relation between the old and the new basis of states on the dot is summarized in Fig. 4 where $|0\rangle_\lambda$ denotes the vacuum state of slave bosons and parafermions. The use of slave bosons in this paper differs substantially from most works based on slave bosons. In fact, we are interested in the weak-coupling regime (above the Kondo temperature) and not in describing the Kondo crossover. The precise identification between operators is given by

$$d_\sigma = b_0^\dagger f_\sigma + \sigma f_{-\sigma}^\dagger b_2, \tag{44}$$

ensuring the anticommutation relation $d_\uparrow^\dagger d_\downarrow^\dagger + d_\downarrow^\dagger d_\uparrow^\dagger = 0$.

Clearly, this operation enlarges the Hilbert space by adding unphysical states. The set of physical states is thus recovered by imposing the constraint

$$b_2^\dagger b_2 + b_0^\dagger b_0 + \sum_\sigma f_\sigma^\dagger f_\sigma = 1, \tag{45}$$

which commutes with the Hamiltonian. In this basis, the Hamiltonian takes the form $H_{\rm AM} = H_0 + H_c + H_T$, where

$$H_0 = \sum_{k\sigma} \varepsilon_k c_{k\sigma}^\dagger c_{k\sigma} + (\varepsilon_d + \lambda) \sum_\sigma f_\sigma^\dagger f_\sigma, \tag{46a}$$

$$H_C = \lambda b_0^\dagger b_0 + (2\varepsilon_d + U + \lambda) b_2^\dagger b_2, \tag{46b}$$

$$H_T = t \sum_{k\sigma} (c_{k\sigma}^\dagger b_0^\dagger f_\sigma + f_\sigma^\dagger b_0 c_{k\sigma}) + t \sum_{k\sigma} \sigma (c_{k\sigma}^\dagger f_{-\sigma}^\dagger b_2 + b_2^\dagger f_{-\sigma} c_{k\sigma}). \tag{46c}$$

The chemical potential λ has been introduced in order to eliminate nonphysical states by imposing the constraint (45). This projection is realized by setting $\lambda \to +\infty$ at the end of calculations.[53,94,95] The key point of the representation of Eq. (46) is that the Hamiltonian is quadratic in the absence of tunneling and standard diagrammatic techniques become applicable. To make more easily contact with the Kondo model, it is convenient to shift the chemical potential $\lambda \to \lambda - \varepsilon_d$.

With the free propagators:

$$G_{k\sigma}^{-1}(i\omega_n) = i\omega_n - \varepsilon_k, \tag{47a}$$

$$F_\sigma^{-1}(i\omega_n) = i\omega_n - \lambda, \tag{47b}$$

$$F_0^{-1}(i\nu_n) = i\nu_n + \varepsilon_d - \lambda, \tag{47c}$$

$$F_2^{-1}(i\nu_n) = i\nu_n - \varepsilon_d - U - \lambda, \tag{47d}$$

where $i\omega_n = (2\pi n + 1)/\beta$ denote always fermionic Matsubara frequencies and $i\nu_n = 2\pi n/\beta$ bosonic ones, the action corresponding to Eq. (46) reads

$$\begin{aligned} S = &- \sum_{i\omega_n k\sigma} c_{k\sigma}^\dagger(i\omega_n) G_{k\sigma}^{-1}(i\omega_n) c_{k\sigma}(i\omega_n) \\ &- \sum_{i\omega_n \sigma} f_\sigma^\dagger(i\omega_n) F_\sigma^{-1}(i\omega_n) f_\sigma(i\omega_n) \\ &- \sum_{i\nu_n} \big[b_0^\dagger(i\nu_n) F_0^{-1}(i\nu_n) b_0(i\nu_n) \\ &+ b_2^\dagger(i\nu_n) F_2^{-1}(i\nu_n) b_2(i\nu_n) \big] \\ &+ \frac{t}{\sqrt{\beta}} \sum_{\substack{i\omega_n i\nu_n \\ k\sigma}} [c_{k\sigma}^\dagger(i\omega_n) b_0^\dagger(i\nu_n) f_\sigma(i\nu_n + i\omega_n) \\ &+ \sigma c_{k\sigma}^\dagger(i\omega_n) f_{-\sigma}^\dagger(i\nu_n - i\omega_n) b_2(i\nu_n) + \text{c.c.}]. \end{aligned} \tag{48}$$

The action being quadratic in the high-energy modes b_0 and b_2, their integration is straightforward and gives an action describing a Kondo model with frequency-dependent couplings

$$\begin{aligned} S' = S_0 + \frac{1}{\beta} \sum_{\substack{kk'\sigma\sigma'\tau\tau' \\ i\omega_1 i\omega_2 i\nu_n}} &(\mathcal{J} \mathbf{S}_{\sigma\sigma'} \cdot \mathbf{s}_{\tau\tau'} + \mathcal{K} \delta_{\sigma\sigma'} \delta_{\tau\tau'}) \\ &\times c_{k\sigma}^\dagger(i\omega_1) c_{k'\sigma'}(i\omega_2) f_\tau^\dagger(i\nu_n + i\omega_2) f_{\tau'}(i\nu_n + i\omega_1), \end{aligned} \tag{49a}$$

$$\mathcal{J} = -2t^2 \left[F_2(i\nu_n + i\omega_1 + i\omega_2) + F_0(i\nu_n) \right], \tag{49b}$$

$$\mathcal{K} = \frac{t^2}{2} \left[F_2(i\nu_n + i\omega_1 + i\omega_2) - F_0(i\nu_n) \right],$$

where S_0 stands for the free action of lead electrons and parafermions.

1. From Anderson to Kondo

We now elaborate on the connection between the action (49), strictly equivalent to the Anderson model, and the Kondo model. The IR limit of the frequency-dependent couplings Eq. (49b) is fixed by the poles of the Green's functions, Eq. (47a) at the Fermi momentum and (47b), i.e., $i\nu_n = \lambda$, $i\omega_1 = i\omega_2 = 0$. In this limit, the couplings $\mathcal{J}$ and $\mathcal{K}$ reproduce exactly the values J and K of Eq. (35) obtained after the Schrieffer-Wolff transformation, and they control operators that are marginal in the RG sense. Expanding the couplings in the frequencies $i\nu_n$, $i\omega_{1/2}$ around the IR limit generates irrelevant operators in the action that we neglect for

the moment. The action now takes the form

$$S = S_0 + \int d\tau \left[J\mathbf{S}(\tau)\cdot\mathbf{s}(\tau) + K\sum_{kk'\sigma} c^\dagger_{k\sigma}(\tau)c_{k'\sigma}(\tau)\hat{n}_f(\tau)\right], \tag{50}$$

with the definitions $\mathbf{S} = \sum_{\sigma\sigma'} f^\dagger_\sigma \frac{\boldsymbol{\tau}_{\sigma\sigma'}}{2} f_{\sigma'}$ and $\hat{n}_f = \sum_\sigma f^\dagger_\sigma f_{\sigma'}$ ($\mathbf{s}$ is the local spin operator for lead electrons defined in Sec. III B 1). The limit $\lambda \to +\infty$ now enforces $\hat{n}_f = 1$ and, using the spin representation by Abrikosov,[95] we recognize the action Eq. (50) as corresponding exactly to the Kondo Hamiltonian given by Eq. (34). We thus recover the same result as the Schrieffer-Wolff transformation in Sec. III B 1.

The irrelevant frequency dependencies in the couplings Eq. (49b) die out upon lowering the cutoff Λ well below U, ε_d and do not change the low-energy Kondo form Eq. (50). However, along the transient region where they still exist, they can weakly renormalize the value of the constants J and K. This generates a perturbative expansion of J and K in powers of Γ/U where the leading order is given by the Schrieffer-Wolff results of Eq. (35).

In order to derive this expansion, we compute the renormalized vertex $\mathcal{V}^R(\Lambda) = \mathcal{Z}(\Lambda)\mathcal{V}(\Lambda)$, where $\mathcal{V}(\Lambda)$ is the bare vertex and $\mathcal{Z}(\Lambda)$ the quasiparticle weight of the parafermion propagator. Both quantities, to be defined more precisely below, depend on the running energy scale Λ. From works on the multiplicative RG approach to the Kondo model, it is known that the RG flow in the Kondo model is fully encoded in the functional dependence of $\mathcal{V}^R$ on Λ.[95–97] The strategy is thus to compute $\mathcal{V}^R(\Lambda)$ in the Anderson model, or equivalently, from the action Eq. (49), at intermediate energy $T_K \ll \Lambda \ll U, |\varepsilon_d|$ in which case the functional dependence of $\mathcal{V}^R$ on Λ is expected to match the Kondo one. A comparison of this calculation with the known expression for $\mathcal{V}^R(\Lambda)$ in the Kondo model identifies the values of J K, and the cutoff D that characterize the effective Kondo Hamiltonian (34) [or Eq. (50)] for the Anderson model at intermediate energy.

2. The parafermion propagator

We introduce the parafermion propagator $\mathcal{F}_\sigma(\tau - \tau') = -\langle \mathcal{T}_\tau f_\sigma(\tau) f^\dagger_\sigma(\tau')\rangle$, where $\mathcal{T}_\tau$ denotes time ordering. In frequency space, the bare propagator (47b) is modified by the self-energy

$$\mathcal{F}_\sigma(i\omega_n) = \frac{1}{i\omega_n - \lambda - \Sigma_\sigma(i\omega_n)}. \tag{51}$$

Following Solyom's prescription,[98] the vertex $\mathcal{V}(\Lambda)$ is calculated for equal incoming and outgoing frequencies together with the analytical continuation

$$i\omega \to 0 \quad \text{for lead electrons,} \tag{52a}$$
$$i\omega_\Lambda \to \tilde{\varepsilon}_d - \Lambda \quad \text{for parafermions.} \tag{52b}$$

Λ is the running energy scale of the RG flow that plays the role of an IR cutoff in vertex calculations. $\tilde{\varepsilon}_d$ is the renormalized single-level energy of the dot obtained from the pole of the parafermion propagator (51), or

$$\tilde{\varepsilon}_d = \lambda + \mathrm{Re}\Sigma(\tilde{\varepsilon}_d), \tag{53}$$

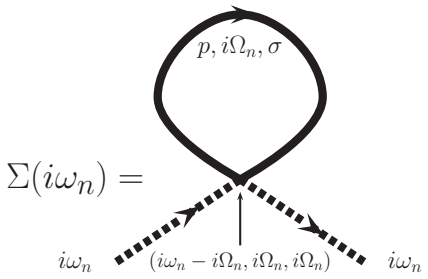

FIG. 5. Self-energy of the parafermion propagator to first order Γ.

while the residue at the pole defines the quasiparticle weight $\mathcal{Z}(\Lambda)$. Its dependence on Λ can be neglected, $\mathcal{Z}(\Lambda) \simeq \mathcal{Z}_0$, as long as $\Lambda \ll \max(-\varepsilon_d, U + \varepsilon_d)$. This last assumption is nevertheless only valid within the precision of our perturbative calculation (second order in Γ) where no IR divergence appears in $\mathcal{Z}(\Lambda)$. Close to its pole, the parafermion propagator takes the form

$$\mathcal{F}_\sigma(i\omega_n) = \frac{\mathcal{Z}_0}{i\omega_n - \tilde{\varepsilon}_d}, \tag{54}$$

with $\mathcal{Z}_0 = [1 - \partial_\omega \Sigma(\tilde{\varepsilon}_d)]^{-1}$.

The self-energy $\Sigma_\sigma(i\omega_n)$ is computed to first order in Γ to be consistent with our overall second order calculation. The corresponding diagram is shown in Fig. 5 with the expression

$$\begin{aligned}\Sigma(i\omega_n) &= \frac{2}{\beta}\sum_{k,i\Omega_n} G_k(i\Omega)\mathcal{K}(i\omega_n - i\Omega_n, i\Omega_n, i\Omega_n)\\ &= t^2\sum_k \left[\frac{f(\varepsilon_k) + b(\varepsilon_d + U + \lambda)}{i\omega_n + \varepsilon_k - \varepsilon_d - U - \lambda}\right.\\ &\quad \left. - \frac{f(\varepsilon_k) + b(-\lambda + \varepsilon_d)}{i\omega_n - \varepsilon_k - \lambda + \varepsilon_d}\right].\end{aligned} \tag{55}$$

The limit $\lambda \to \infty$ is taken and the result reads, after summation over the energies of the lead electrons,

$$\Sigma(i\omega_n) = \frac{\Gamma}{\pi}\left(\ln\frac{\varepsilon_d + U + \lambda - i\omega_n}{D_0} + \ln\frac{\lambda - \varepsilon_d - i\omega_n}{D_0}\right). \tag{56}$$

An intermediate cutoff noted D_0 has been introduced here to remove ultraviolet (UV) divergences. However, as we shall see, D_0 plays no role and disappears from the final results. Eq. (53) for $\tilde{\varepsilon}_d$ can be solved perturbatively. To first order in Γ, one finds

$$\tilde{\varepsilon}_d = \lambda + \frac{\Gamma}{\pi}\left(\ln\frac{\varepsilon_d + U}{D_0} + \ln\frac{-\varepsilon_d}{D_0}\right). \tag{57}$$

After standard analytical continuation, the quasiparticle weight is also extracted from Eq. (56):

$$\mathcal{Z}_0 = 1 - \nu_0 t^2\left(\frac{1}{\varepsilon_d + U} - \frac{1}{\varepsilon_d}\right) = 1 - \frac{\nu_0}{2}J_0. \tag{58}$$

J_0 is the Schrieffer-Wolff result, Eq. (35a), for J.

3. The vertex

The vertex $\mathcal{V}(\Lambda)$ is given by the series of irreducible diagrams drawn in Fig. 6. The calculation is performed up

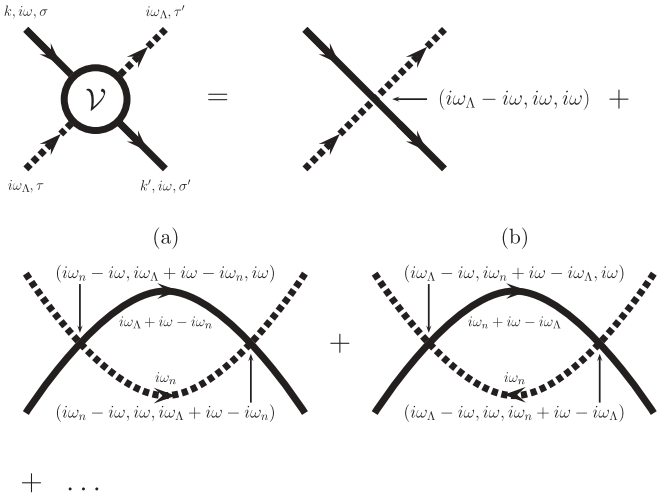

FIG. 6. Diagrammatic series for the vertex $\mathcal{V}$.

to second order in Γ, or fourth order in t. The leading order is the bare vertex shown in Fig. 7 which, after the analytical continuation of Eqs. (52), reproduces the Schrieffer-Wolff expression

$$\mathcal{V}(\Lambda) = \mathcal{V}_1 = \mathbf{S}_{\tau'\tau} \cdot \mathbf{s}_{\sigma'\sigma} J_0 + \delta_{\tau\tau'}\delta_{\sigma\sigma'} K_0, \tag{59}$$

with the coupling constants of Eqs. (35a) and (35b). In order to derive Eq. (59), we have used that $\tilde{\varepsilon}_d = \lambda$ to leading order and discarded $\Lambda/\max(-\varepsilon_d, U + \varepsilon_d)$ corrections.

The renormalized vertex $\mathcal{V}^R(\Lambda)$ splits as

$$\mathcal{V}^R = \mathcal{V}_1 + \mathcal{V}_Z + \mathcal{V}^a + \mathcal{V}^b, \tag{60}$$

where $\mathcal{V}_Z$ and $\mathcal{V}^{a,b}$ are second order terms in Γ. $\mathcal{V}_Z$ collects the corrections to $\mathcal{V}_1$ in the bare vertex of Fig. 7 brought by the quasiparticle weight $\mathcal{Z}_0$ of Eq. (58) and the renormalization of the single-level energy (57). It contains exchange and potential scattering terms

$$\mathcal{V}_Z = \mathbf{S} \cdot \mathbf{s} \nu_0 \left[\left(\frac{J_0^2}{4} + 4K_0^2 \right) \left(\ln \frac{-\varepsilon_d(\varepsilon_d + U)}{D_0^2} \right) - \frac{J_0^2}{2} \right] + \delta_{\tau\tau'}\delta_{\sigma\sigma'} \nu_0 \frac{J_0 K_0}{2} \left[\ln \frac{-\varepsilon_d(\varepsilon_d + U)}{D_0^2} - 1 \right]. \tag{61}$$

The vertex corrections $\mathcal{V}^{a,b}$ are illustrated in Fig. 6. The first one (a) takes the form

$$\mathcal{V}^a = -\frac{1}{\beta} \sum_{k, i\omega_n} F_\sigma(i\omega_n) G_k(i\omega_\Lambda + i\omega - i\omega_n) \times \left[\mathbf{S}_{\beta\tau} \cdot \mathbf{s}_{\alpha\sigma} \mathcal{J}_{i\omega_n - i\omega, i\omega_\Lambda + i\omega - i\omega_n, i\omega} + \delta_{\beta\tau}\delta_{\alpha\sigma} \mathcal{K}_{i\omega_n - i\omega, i\omega_\Lambda + i\omega - i\omega_n, i\omega} \right] \times \left[\mathbf{S}_{\tau'\beta} \cdot \mathbf{s}_{\sigma'\alpha} \mathcal{J}_{i\omega_n - i\omega, i\omega, i\omega_\Lambda + i\omega - i\omega_n} + \delta_{\beta\tau'}\delta_{\alpha\sigma'} \mathcal{K}_{i\omega_n - i\omega, i\omega, i\omega_\Lambda + i\omega - i\omega_n} \right]. \tag{62}$$

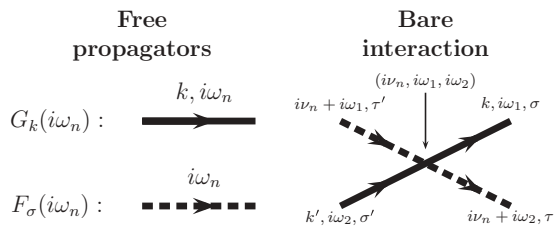

FIG. 7. (Left) Free propagators of the theory. (Right) Bare interaction of the theory. The frequencies inside the parenthesis are the arguments of the frequency-dependent couplings in Eq. (49b).

The overall minus comes from diagrammatic rules and the Einstein convention is used for spin summation. The calculation of this vertex correction is carried out in Appendix A. We find $\mathcal{V}^a = \mathcal{V}_J^a \, \mathbf{S} \cdot \mathbf{s} + \mathcal{V}_K^a$ with

$$\mathcal{V}_J^a = -4\nu_0 t^4 \left[\frac{1}{(\varepsilon_d + U)^2} \ln \frac{\Lambda}{D_0} + \frac{1}{\varepsilon_d(\varepsilon_d + U)} \left(\ln \frac{-\varepsilon_d}{D_0} - \ln \frac{\Lambda}{D_0} \right) \right], \tag{63a}$$

$$\mathcal{V}_K^a = \nu_0 t^4 \left[\frac{1}{\varepsilon_d^2} \left(1 - \ln \frac{-\varepsilon_d}{D_0} + \ln \frac{\Lambda}{D_0} \right) + \frac{1}{\varepsilon_d(\varepsilon_d + U)} \times \left(\ln \frac{-\varepsilon_d}{D_0} - \ln \frac{\Lambda}{D_0} \right) + \frac{1}{(\varepsilon_d + U)^2} \ln \frac{\Lambda}{D_0} \right]. \tag{63b}$$

The calculation of the (b) diagram follows exactly the same steps:

$$\mathcal{V}^b = -\frac{1}{\beta} \sum_{k, i\omega_n} F_\sigma(i\omega_n) G_k(i\omega_n + i\omega - i\omega_\Lambda) \times \left[\mathbf{S}_{\tau'\beta} \cdot \mathbf{s}_{\alpha\sigma} \mathcal{J}_{i\omega_\Lambda - i\omega, i\omega_n + i\omega - i\omega_\Lambda, i\omega} + \delta_{\beta\tau'}\delta_{\alpha\sigma} \mathcal{K}_{i\omega_\Lambda - i\omega, i\omega_n + i\omega - i\omega_\Lambda, i\omega} \right] \times \left[\mathbf{S}_{\beta\tau} \cdot \mathbf{s}_{\sigma'\alpha} \mathcal{J}_{i\omega_\Lambda - i\omega, i\omega, i\omega_n + i\omega - i\omega_\Lambda} + \delta_{\beta\tau}\delta_{\alpha\sigma'} \mathcal{K}_{i\omega_\Lambda - i\omega, i\omega, i\omega_n + i\omega - i\omega_\Lambda} \right], \tag{64}$$

and also contains exchange and potential scattering terms:

$$\mathcal{V}_J^b = -4\nu_0 t^4 \left[\frac{1}{\varepsilon_d^2} \ln \frac{\Lambda}{D_0} + \frac{1}{\varepsilon_d(\varepsilon_d + U)} \left(\ln \frac{\varepsilon_d + U}{D_0} - \ln \frac{\Lambda}{D_0} \right) \right], \tag{65a}$$

$$\mathcal{V}_K^b = -\nu_0 t^4 \left[\frac{1}{(\varepsilon_d + U)^2} \left(1 + \ln \frac{\Lambda}{D_0} - \ln \frac{\varepsilon_d + U}{D_0} \right) + \frac{1}{\varepsilon_d(\varepsilon_d + U)} \left(\ln \frac{\varepsilon_d + U}{D_0} - \ln \frac{\Lambda}{D_0} \right) + \frac{1}{\varepsilon_d^2} \ln \frac{\Lambda}{D_0} \right]. \tag{65b}$$

Adding the results from Eqs. (59), (61), (63), and (65), the renormalized vertex $\mathcal{V}^R(\Lambda) = \mathcal{V}_J(\Lambda) \, \mathbf{S} \cdot \mathbf{s} + \mathcal{V}_K(\Lambda)$ expands as

$$\mathcal{V}_J = J_0 - \frac{\nu_0}{2} J_0^2 - \nu_0 J_0^2 \ln \left[\frac{\Lambda}{\sqrt{-\varepsilon_d(\varepsilon_d + U)}} \right], \tag{66a}$$

$$\mathcal{V}_K = K_0 + \frac{\nu_0}{2} J_0 \, K_0 + \frac{\nu_0}{8} J_0^2 \ln \left(\frac{\varepsilon_d + U}{-\varepsilon_d} \right). \tag{66b}$$

As anticipated, D_0 has disappeared from these final expressions and the charging energy $\sqrt{-\varepsilon_d(\varepsilon_d + U)}$ acts as an effective high-energy cutoff. Remarkably, the IR cutoff Λ also disappears from the expression of the potential scattering term $\mathcal{V}_K$ where the limit $\Lambda \to 0$ can safely be taken. However, the $\ln \Lambda$ dependence in $\mathcal{V}_J$ signals the onset of the Kondo singularity which develops at low energy and restricts the

validity of Eqs. (66) to the energy window $T_K \ll \Lambda \ll \sqrt{-\varepsilon_d(\varepsilon_d+U)}$.

In agreement with the leading order calculation of Sec. III B 1, $\mathcal{V}_K$ vanishes at the particle-hole symmetric point $\varepsilon_d = -U/2$. This property is, in fact, expected by symmetry to hold to all orders in Γ.

4. Kondo temperature and charge susceptibility

In order to test our predictions, see Eq. (66), we compare them to existing results from the literature. We show that Eq. (66) give access for the Anderson model to the Kondo temperature and the static charge susceptibility. Our expression for the Kondo temperature reproduces a standard result due to Haldane and the charge susceptibility agrees with a Bethe-ansatz calculation at the particle-hole symmetric point. These successful comparisons validate our approach.

Let us first consider the Kondo model (34) characterized by the exchange coupling J and the high-energy cutoff (bandwidth) D, with no potential scattering. In the Wilsonian language, the RG flow corresponds to integrating the model continuously over high-energy states, thereby reducing the cutoff from D to Λ and changing the exchange coupling constant from J to $\mathcal{V}_J^{\rm Kondo}(\Lambda)$. Hence two Kondo models are equivalent if the RG flow connects them even if their bare values of J and D are different. $\mathcal{V}_J^{\rm Kondo}(\Lambda)$ can be calculated by different means, but in the field theory language with Abrikosov parafermions,[95,99] it is defined from the same renormalized vertex as the one used in this paper and illustrated in Fig. 6. The one-loop calculation gives[88,98]

$$\mathcal{V}_J^{\rm Kondo}(\Lambda) = J - \nu_0 J^2 \ln\frac{\Lambda}{D} + \cdots. \tag{67}$$

We already gave RG arguments in Sec. III C 1 showing that the Anderson model maps exactly onto the Kondo model for energies well below the charging energy $\sqrt{-\varepsilon_d(\varepsilon_d+U)}$. The identification between Eqs. (67) and (66a) thus determines the coupling constants J and D for the Kondo model, inherited from the Anderson model, in terms of the original parameters t, ε_d, and U. With the arbitrary choice

$$D = \sqrt{-\varepsilon_d(\varepsilon_d+U)}, \tag{68}$$

Eq. (67) is reproduced from Eq. (66a) if $J = J_0 - (\nu_0/2)J_0^2$ or

$$\nu_0 J = -\frac{2\Gamma\, U}{\pi\,\varepsilon_d(\varepsilon_d+U)} - \frac{2\Gamma^2\, U^2}{\pi^2\varepsilon_d^2(\varepsilon_d+U)^2}. \tag{69}$$

The Kondo temperature T_K is the energy scale for which $\mathcal{V}_J^{\rm Kondo}(T_K)$ is of order one. Among the different definitions of T_K, we use the high-temperature $T \gg T_K$ expansion[100] of the spin susceptibility (in proper units)

$$\chi(T) = \frac{1}{4\,T}\left\{1 - \frac{1}{\ln(T/T_K)} - \frac{1}{2}\frac{\ln[\ln(T/T_K)]}{(\ln T/T_K)^2}\right\}. \tag{70}$$

A two-loop perturbative RG calculation on the Kondo model (34) gives the Kondo temperature[68]

$$T_K = \mathcal{B}\, D\sqrt{\nu_0\, J}\, e^{-1/\nu_0 J}, \tag{71}$$

depending on J and D, where $\mathcal{B}$ is a prefactor of order one. The precise value, $\mathcal{B} = e^{\frac{3}{4}+C}/2\pi$ where $C = 0.5772\ldots$ is Euler's constant, is obtained by comparing Eq. (70) with a weak coupling (in J) calculation of the susceptibility.[68,101] Substituting J and D in the Kondo temperature (71) by their expressions Eqs. (68) and (69) in terms of the parameters of the Anderson model, the formula (30) derived by Haldane using a completely different approach[90] is recovered.

So far in this discussion, we have discarded the potential scattering term in Eq. (34) because it does not alter the RG flow and the results of Eqs. (68), (69), and (30) are still valid. The potential scattering term can in fact be absorbed[86–88] into a redefinition of the lead electron wave functions (with a minor negligible correction as discussed in Sec. III B 1) such that the standard Kondo RG flow is recovered, albeit with electrons scattered with the phase shift $\delta_\sigma - \pi/2 = -\arctan(\pi\,\nu_0 K(\varepsilon_d)) \simeq -\pi\,\nu_0 K(\varepsilon_d)$ with respect to the original electrons. Here, $K(\varepsilon_d) = \mathcal{V}_K^b$, see Eq. (65b). Using the Friedel sum rule $\sum_\sigma \delta_\sigma = \pi\,\langle\hat{n}\rangle$, the dot occupancy reads $\langle\hat{n}\rangle = 1 - 2\nu_0 K(\varepsilon_d)$ leading, for the charge susceptibility, to the formula Eq. (29) previously advertised. In the particle-hole symmetric case, Eq. (29) reduces to

$$\chi_c = \frac{8\Gamma}{\pi U^2}\left[1 + \frac{6}{\pi}\left(\frac{2\Gamma}{U}\right)\right], \tag{72}$$

in agreement with a Bethe ansatz calculation.[89]

With Eq. (29), we show that the charge fluctuations in the Anderson model can be calculated perturbatively despite the Kondo singularity that affects only the spin fluctuations. This is another indication of the spin/charge separation in the Anderson model.[102] This separation no longer occurs in the presence of a magnetic field and the problem of charge fluctuations becomes nonperturbative. Nevertheless, the Fermi liquid approach discussed in Sec. II still applies to the finite magnetic field case.[71]

D. Field theory approach II: Renormalization of the Coulomb blockade model

Unlike the Anderson model, the CBM does not exhibit logarithmic singularities and the derivation of the low-energy effective model can be performed using perturbation theory. Nevertheless, similarly to the Anderson model, an expansion of the CBM Hamiltonian Eq. (3) around the zero tunneling limit $t = 0$ is unworkable because the unperturbed Hamiltonian is not quadratic and Wick's theorem does not apply. We thus extend the approach of Barnes by introducing one boson operator b_n for each charge state with exactly n electrons on the dot. The projection onto the physical sector

$$\sum_n b_n^\dagger b_n = 1 \tag{73}$$

is realized with the chemical potential λ, as in Sec. III C, taken to infinity at the end of calculations. In this new basis, the number of electrons on the dot is $\hat{n} = \sum_n n\, b_n^\dagger b_n$ and the charging energy part of the Hamiltonian Eq. (3) reads $H_c = E_c \sum_n n^2\, b_n^\dagger b_n$. The charge states are coupled by the tunneling term

$$H_T = t\sum_{kl\sigma}(d_{l\sigma}^\dagger c_{k\sigma}\mathcal{A}^\dagger + c_{k\sigma}^\dagger d_{l\sigma}\mathcal{A}), \tag{74}$$

where the operator $\mathcal{A} = \sum_n b^\dagger_{n-1} b_n$ removes one electron from the dot.

With $-E_c < \varepsilon_d < E_c$, $n = 0$ defines the low-energy sector and, in a second order expansion in the dimensionless conductance $g = N(\nu_0 t)^2$, only the charge states $n = \pm 1, \pm 2$ are virtually occupied. We thus discard all charge states with $|n| > 2$ from the action. The action assumes the form $S = S_0 + S_1$ with

$$S_0 = \mathrm{Tr}\left(-\sum_{k\sigma} c^\dagger_{k\sigma} G_k^{-1} c_{k\sigma} - \sum_{l\sigma} d^\dagger_{l\sigma} D_l^{-1} d_{l\sigma} \right), \tag{75a}$$

$$S_1 = \mathrm{Tr}\left[-\sum_{n=-2}^{2} b^\dagger_n F_n^{-1} b_n + t \sum_{kl\sigma} (c^\dagger_{k\sigma} d_{l\sigma} \mathcal{A} + d^\dagger_{l\sigma} c_{k\sigma} \mathcal{A}^\dagger) \right], \tag{75b}$$

where the trace stands for the typical integral over imaginary time

$$\mathrm{Tr}\,(O) = \int_0^\beta d\tau\, O(\tau). \tag{76}$$

The free propagators are given by

$$G_k^{-1} = -\partial_\tau - \varepsilon_k, \tag{77a}$$

$$D_l^{-1} = -\partial_\tau - \varepsilon_l, \tag{77b}$$

$$F_n^{-1} = -\partial_\tau - \lambda - E_n, \tag{77c}$$

where $E_n = E_c n^2 + \varepsilon_d n$ denote the bare energies of the charge states.

The structure of the action (75) allows the straightforward integration of the high-energy fields $b_{\pm 1}$ and $b_{\pm 2}$ as detailed in Appendix B. The action then reads $S' = S_0 + S_2$, where

$$S_2 = \mathrm{Tr}\left[-b_0^\dagger F_0^{-1} b_0 + t^2 \sum_{\substack{kk'll' \\ \sigma\sigma'}} (c^\dagger_{k\sigma} d_{l\sigma} b_0^\dagger F_1 d^\dagger_{l'\sigma'} c_{k'\sigma'} b_0 + d^\dagger_{l\sigma} c_{k\sigma} b_0^\dagger F_{-1} c^\dagger_{k'\sigma'} d_{l'\sigma'} b_0) + t^4 \sum_{\substack{kk'k''k'''ll'l''l''' \\ \sigma\sigma'\sigma''\sigma'''}} c^\dagger_{k\sigma} d_{l\sigma} b_0^\dagger F_1 c^\dagger_{k''\sigma''} d_{l''\sigma''} \right.$$
$$\left. \times\, F_2 d^\dagger_{l'''\sigma'''} c_{k'''\sigma'''} F_1 d^\dagger_{l'\sigma'} c_{k'\sigma'} b_0 + t^4 \sum_{\substack{kk'k''k'''ll'l''l''' \\ \sigma\sigma'\sigma''\sigma'''}} d^\dagger_{l\sigma} c_{k\sigma} b_0^\dagger F_{-1} d^\dagger_{l''\sigma''} c_{k''\sigma''} F_{-2} c^\dagger_{k'''\sigma'''} d_{l'''\sigma'''} F_{-1} c^\dagger_{k'\sigma'} d_{l'\sigma'} b_0 \right]. \tag{78}$$

This action is the starting point of our perturbative expansion around $t = 0$. The unperturbed action for $t = 0$ is indeed quadratic and standard diagrammatics is applicable. Switching to the frequency representation of the trace, the bare interaction of the theory can be drawn diagrammatically as in Fig. 8. In this section, we use the Wilsonian RG approach and introduce the running energy scale Λ in the decomposition $\phi = \phi^s + \phi^f$, where $\phi = b_0, c_k, d_l$. ϕ^s represents the slow degrees of freedom with Matsubara frequencies $\omega_n < \Lambda$ and ϕ^f the fast ones, $\omega_n > \Lambda$, that are integrated after expanding the action Eq. (78) around $t = 0$. In the diagrams shown in Figs. 9–12, the external lines are slow modes and the internal lines fast modes. In the standard RG treatment, the integration over fast modes is realized continuously to follow the evolution of the coupling constants under RG. This is not necessary in our case since no IR divergence occurs in diagrams. The fast modes are therefore integrated all at once and, since we are interested in the low-energy limit $\Lambda \to 0$, the energy windows for the fast modes in fact extends over all frequencies.

1. Low-energy theory

After averaging over the fast modes and re-exponentiating the action, one obtains the low-energy form

$$S = S_0 + \int_0^\beta d\tau \left\{ -b_0^\dagger(\tau) \mathcal{F}_0^{-1} b_0(\tau) + \mathcal{V} \sum_{kk'\sigma} [c^\dagger_{k\sigma}(\tau) c_{k'\sigma}(\tau) - d^\dagger_{k\sigma}(\tau) d_{k'\sigma}(\tau)] b_0^\dagger(\tau) b_0(\tau) \right\}, \tag{79}$$

where $\mathcal{F}_0$ stands for the full propagator of the slave boson b_0. The opposite sign of the lead and dot scattering terms originates from the ordering of the operators in Eq. (78). The

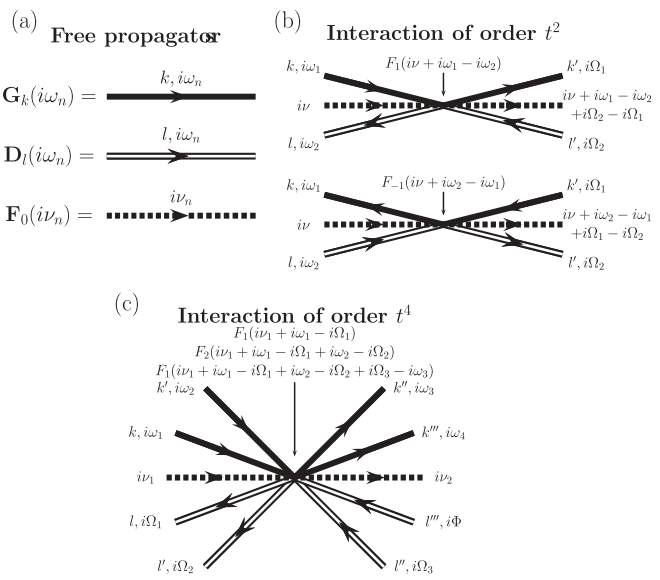

FIG. 8. Diagrammatic representation of free propagators in the CBM integrated action (a). The diagrams are represented in the frequency domain. The bare interaction of order t^2 (b) and the one of order t^4 (c) are also shown. $i\Phi = i\Omega_1 - i\omega_1 - i\nu_1 + i\Omega_2 - i\omega_2 + i\omega_3 - i\Omega_3 + i\omega_4 + i\nu_2$. The arrows pointing to the center of these vertices indicate the frequency dependence of the high-energy propagators included in the interaction (78).

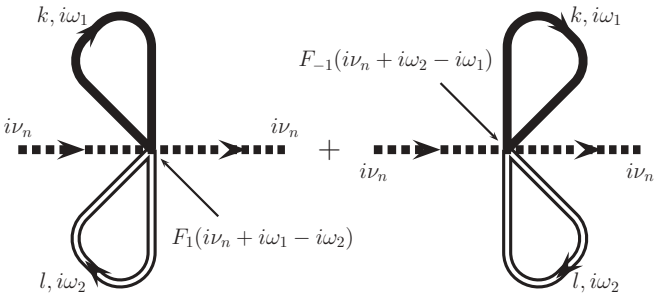

FIG. 9. First-order diagrams for the slave-boson self-energy.

pole of the slave-boson propagator (recall that $E_0 = 0$)

$$\mathcal{F}_0(i\nu_n) = \frac{1}{i\nu_n - \lambda - \Sigma_0(i\nu_n)} \tag{80}$$

defines the renormalized slave-boson energy $\tilde{E}_0 = \lambda + \Sigma_0(\tilde{E}_0)$. Close to this pole, the self-energy $\Sigma_0(i\nu_n)$ is regular and the slave-boson propagator takes the form

$$\mathcal{F}_\sigma(i\nu_n) = \frac{\mathcal{Z}_0}{i\nu_n - \tilde{E}_0}, \tag{81}$$

with $\mathcal{Z}_0 = [1 - \partial_\omega \Sigma_0(\tilde{E}_0)]^{-1}$. Thus the IR fixed point corresponds to $i\nu = \tilde{E}_0$.

The coupling constant $\mathcal{V}$ in the action Eq. (79) derives from the interaction vertex between slave-bosons and lead fermions ($-\mathcal{V}$ for the dot fermions), illustrated in Fig. 10 to lowest order in g, taken at $i\nu = \tilde{E}_0$ for the slave-bosons and $i\omega = 0$ for the fermions. A rescaling of the slave-boson field $b_0 \to \sqrt{\mathcal{Z}_0}\, b_0$ in Eq. (79) removes $\mathcal{Z}_0$ from the propagator (81) and renormalizes the vertex $\mathcal{V} \to \mathcal{V}^R$. The renormalized vertex $\mathcal{V}^R$ is therefore the relevant object describing the scattering of electrons as in Sec. III C for the Anderson model. After this rescaling, the limit $\lambda \to +\infty$ simply enforces $b_0^\dagger(\tau) b_0(\tau) = 1$ and the low-energy Hamiltonian corresponding to the action (79) becomes

$$H = H_0 + \mathcal{V}^R \sum_{kk'\sigma} (c_{k\sigma}^\dagger c_{k'\sigma} - d_{k\sigma}^\dagger d_{k'\sigma}) \tag{82}$$

and confirms the Fermi liquid picture developed in Sec. II E, see for instance Eq. (14) with $K(\varepsilon_d) = \pm\mathcal{V}_R$ for the lead/dot electrons.

Sections III D 2 and III D 3 are devoted to the evaluation of $\mathcal{V}^R$. The slave-boson propagator is first calculated, in order to access $\mathcal{Z}_0$ and $\tilde{E}_0$, then the vertex $\mathcal{V}$. We finally apply the Friedel sum rule to the Hamiltonian (82) to determine the mean occupancy of the dot and compare with a direct calculation.

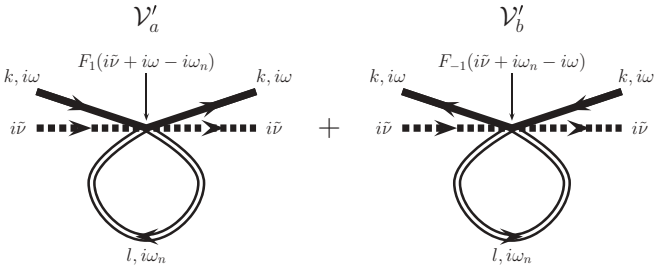

FIG. 10. First-order diagrams for the vertex $\mathcal{V}$.

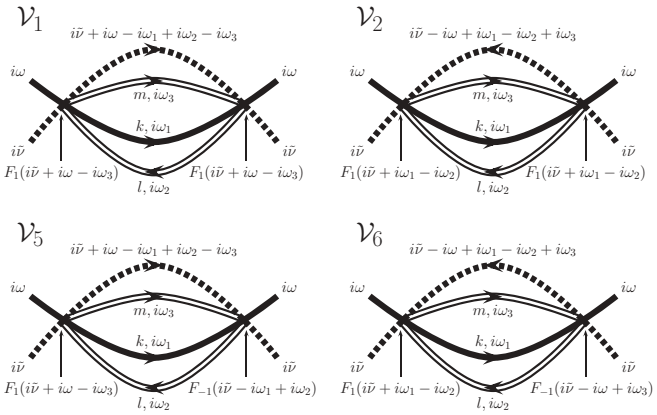

FIG. 11. Second-order (in g) diagrams involving the six-leg vertex shown in Fig. 8 and scaling as Nt^4. The diagrams corresponding to the contributions $\mathcal{V}_3$ and $\mathcal{V}_4$ are not shown, they are similar to $\mathcal{V}_1$ and $\mathcal{V}_2$ but come with an opposite sign and the change $E_n \to E_{-n}$, see also Appendix C. The diagrams scaling only as t^4 have been discarded under the assumption of large channel number N.

2. The slave-boson propagator

For an overall calculation of second order in g, only the first-order approximation of the slave-boson self-energy is needed. Including the diagrams shown in Fig. 9, it reads

$$\begin{aligned}\Sigma_0(i\nu_n) &= -\frac{t^2}{\beta^2} \sum_{kl\sigma i\omega_{1,2}} G_k(i\omega_1) D_l(i\omega_2) [F_1(i\nu_n + i\omega_1 - i\omega_2) \\ &\quad + F_{-1}(i\nu_n + i\omega_2 - i\omega_1)] \\ &= -N(\nu_0 t)^2 \int d\varepsilon_1 d\varepsilon_2 \left[\frac{\theta(\varepsilon_1)\theta(\varepsilon_2)}{\varepsilon_1 + \varepsilon_2 + E_1 + \lambda - i\nu_n} \right. \\ &\quad \left. + \frac{\theta(\varepsilon_1)\theta(\varepsilon_2)}{\varepsilon_1 + \varepsilon_2 + E_{-1} + \lambda - i\nu_n} \right],\end{aligned} \tag{83}$$

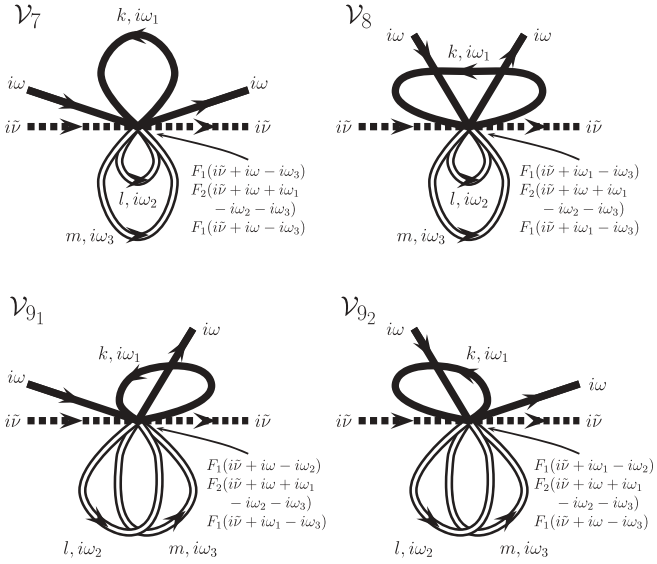

FIG. 12. Same as Fig. 11 but with diagrams involving the ten-leg vertex shown in Fig. 8. The diagrams leading to $\mathcal{V}_{10,11,12}$ are not represented, they are similar to $\mathcal{V}_{7,8,91}$ but come with an opposite sign and the change $E_n \to E_{-n}$, see also Appendix C. Notice $\mathcal{V}_9 = \mathcal{V}_{91} + \mathcal{V}_{92} = 2\mathcal{V}_{91}$.

where all electrons energies have been summed over and the limit $\lambda \to \infty$ taken. The self-energy in Eq. (83) exhibits a linear UV divergence. The theory is regularized with the cutoff function $e^{-\varepsilon/D_0}$. Fortunately, all UV divergences cancel out in the final expression of the renormalized vertex, as discussed in Appendix C and the limit $D_0 \to +\infty$ is eventually taken. From Eq. (83), one extracts the values of $\mathcal{Z}_0 = 1 + \partial_\omega \Sigma_0(\lambda)$ and the renormalized energy $\tilde{E}_0 = \lambda + \Sigma_0(\lambda)$ to order g.

3. The vertex

The leading contributions to the vertex $\mathcal{V}$ are represented in Fig. 10. They are similar to the self-energy diagrams of Fig. 9 but without contraction of the lead electron lines. The first diagram gives

$$\begin{aligned} &-\frac{t^2}{\beta}\sum_{l,i\omega_n} D_l(i\omega_n) F_1(i\nu + i\omega - i\omega_n) \\ &\quad = -\nu_0 t^2 \int d\varepsilon \frac{1-f(\varepsilon)}{\varepsilon + E_1 - \Sigma(\lambda)}, \\ &\qquad -\frac{t^2}{\beta}\sum_{l,i\omega_n} D_l(i\omega_n) F_1(i\tilde{\nu} + i\omega - i\omega_n) \\ &\quad = -\nu_0 t^2 \int d\varepsilon \frac{1-f(\varepsilon)}{\varepsilon + E_1 - \Sigma(\lambda)}, \end{aligned} \tag{84}$$

where the analytical continuations $i\omega \to 0$ and $i\nu \to \lambda + \Sigma_0(\lambda)$ have been carried out together with the $\lambda \to \infty$ limit. Adding both diagrams in Fig. 10 and expanding to second order in g (fourth in t), we obtain

$$\begin{aligned} \mathcal{V}' = \nu_0 t^2 \ln\frac{E_1}{E_{-1}} + N\nu_0^3 t^4 \int_{\varepsilon_1,\varepsilon_2,\varepsilon_3>0} d\varepsilon_1 d\varepsilon_2 d\varepsilon_3 \\ \times \left(\sum_{s=\pm1} \frac{1}{\varepsilon_1+\varepsilon_2+E_s}\right)\left[\sum_{s=\pm1}\frac{s}{(\varepsilon_3+E_s)^2}\right]. \end{aligned} \tag{85}$$

The number of integration variables is reduced by changing variables, $\varepsilon_1 + \varepsilon_2 \to \varepsilon_1$ and integrating over ε_2, leading to

$$\begin{aligned} \mathcal{V}' = \nu_0 t^2 \ln\frac{E_1}{E_{-1}} + N\nu_0^3 t^4 \int_{\varepsilon_1,\varepsilon_3>0} d\varepsilon_1 d\varepsilon_3 \\ \times \left(\sum_{s=\pm1} \frac{\varepsilon_1}{\varepsilon_1+E_s}\right)\left[\sum_{s=\pm1}\frac{s}{(\varepsilon_3+E_s)^2}\right]. \end{aligned} \tag{86}$$

We note in passing that the leading order result, i.e., the first term in Eq. (86), coincides with our previous Schrieffer-Wolff calculation, see Eq. (41). An additional contribution to the renormalized vertex $\mathcal{V}^R$ is brought by the slave-boson weight $\mathcal{Z}_0$, when the first-order correction to $\mathcal{Z}_0$ multiplies the first term in Eq. (86), namely,

$$\mathcal{V}'' = -N\nu_0^3 t^4 \ln\left(\frac{E_1}{E_{-1}}\right) \int_{\varepsilon>0} d\varepsilon \left[\sum_{s=\pm1}\frac{\varepsilon}{(\varepsilon+E_s)^2}\right]. \tag{87}$$

We finally turn to the genuine second-order diagrams for the vertex $\mathcal{V}$ and therefore $\mathcal{V}^R$. At this point, a distinction can be operated between diagrams scaling as Nt^4 and those scaling as t^4. The calculation is greatly simplified by keeping the former and discarding the latter in a large N calculation. In addition, the diagrams are classified depending on whether they involve the six-leg vertex of Eq. (78) (of order g) shown in Fig. 8, those diagrams being listed in Fig. 11, or the ten-leg vertex (of order g^2), again in Fig. 8, those latter diagrams being listed in Fig. 12.

We shall calculate explicitly only the vertex contribution $\mathcal{V}_1$ and quote the results of other contributions in Appendix C.

The expression associated to the diagram $\mathcal{V}_1$ is given by

$$\begin{aligned} \mathcal{V}_1 = N\frac{t^4}{\beta^3}\sum_{klm,i\omega_{1,2,3}} G_k(-i\omega_1) D_l(i\omega_2) D_m(-i\omega_3) \\ \times F_1^2(i\tilde{\nu}+i\omega+i\omega_3) F_0(i\tilde{\nu}+i\omega+i\omega_1+i\omega_2+i\omega_3), \end{aligned} \tag{88}$$

and, after summing over the Matsubara frequencies $\omega_{1,2,3}$ in the limit $\lambda \to \infty$, one obtains

$$\begin{aligned} \mathcal{V}_1 &= Nt^4 \sum_{klm} \frac{f(-\varepsilon_k) f(\varepsilon_l) f(-\varepsilon_m)}{(\varepsilon_m+E_1)^2(\varepsilon_l-\varepsilon_k-\varepsilon_m)} \\ &= -N\nu_0^3 t^4 \int_{\varepsilon_1,\varepsilon_2>0} d\varepsilon_1 d\varepsilon_2 \frac{\varepsilon_1}{(\varepsilon_2+E_1)^2(\varepsilon_1+\varepsilon_2)}. \end{aligned} \tag{89}$$

The calculation of the other twelve diagrams illustrated in Figs. 11 and 12 are not particularly enlightening and follow the same line as the calculation of $\mathcal{V}_1$. The different contributions are therefore summarized in Appendix C. The summation over these twelve terms together with $\mathcal{V}'$ and $\mathcal{V}''$ is also performed in Appendix C where special attention is paid to the cancellation of the different UV divergences. In the limit $N \to +\infty$, the final result for the renormalized vertex to second order in g reads

$$\mathcal{V}^R = \nu_0 t^2 \ln\frac{E_1}{E_{-1}} + N\nu_0^3 t^4 \left(A[\varepsilon_d] - A[-\varepsilon_d]\right), \tag{90a}$$

$$\begin{aligned} A[\varepsilon_d] = \frac{-\varepsilon_d}{2E_c}\left(\frac{4\pi^2}{3} + \ln^2\frac{E_c+\varepsilon_d}{E_c-\varepsilon_d}\right) \\ + \frac{8\left(2E_c^2 - 2E_c\varepsilon_d - \varepsilon_d^2\right)}{(3E_c+\varepsilon_d)(E_c-\varepsilon_d)} \ln\frac{E_c+\varepsilon_d}{E_c} \\ + \frac{(2E_c+\varepsilon_d)}{E_c}\left[\ln^2\frac{E_c+\varepsilon_d}{4E_c+2\varepsilon_d} + 2Li_2\left(\frac{3E_c+\varepsilon_d}{4E_c+2\varepsilon_d}\right)\right. \\ \left. - \frac{4E_c(2E_c+\varepsilon_d)}{(E_c+\varepsilon_d)(3E_c+\varepsilon_d)} \ln\frac{4E_c+2\varepsilon_d}{E_c}\right]. \end{aligned} \tag{90b}$$

This result, substituted in the low-energy Hamiltonian (82), gives access to the dot occupancy

$$\langle\hat{n}\rangle = g\ln\frac{E_c-\varepsilon_d}{E_c+\varepsilon_d} - g^2\left(A[\varepsilon_d] - A[-\varepsilon_d]\right), \tag{91}$$

by using the Friedel sum rule

$$\langle\hat{n}\rangle = -(N/\pi)\arctan(\pi\nu_0\mathcal{V}^R) \simeq -N\nu_0\mathcal{V}^R.$$

The result of Eq. (91) coincides with a direct calculation of the dot occupancy[78,92] using a different perturbative approach, which validates, at least perturbatively, the Fermi liquid description emphasized in Sec. II.

IV. SUMMARY AND CONCLUSIONS

We investigated the dynamical response of a quantum dot attached to a lead. We studied the low-frequency charge fluctuations on the dot that are related to the admittance of this quantum circuit in the linear regime. We argued that the system at low energy behaves as a local Fermi liquid where inelastic scattering events can be disregarded and lead electrons are simply coherently backscattered by the dot. The present work extends in a way the general analysis built by Büttiker and coworkers to study the dynamic admittance of mesoscopic conductors, by including arbitrarily strong Coulomb interactions within the dot. We avoid the introduction of an approximate self-consistent potential on the dot.

By computing the power dissipated by the external ac drive, we were able to derive a set of general formulas for the quantum capacitance and the charge relaxation resistance that characterize the response of the dot at low frequency. Remarkably, the results are essentially not so different from the weakly interacting picture. The fundamental reason is that electrons close to the Fermi energy do not feel strong interactions as a result of Pauli blocking, following the standard Fermi liquid argument.[75] Our approach is naturally not applicable for models exhibiting non-Fermi liquid physics such as the two-channel model close to charge degeneracy. In these models, the mere definition of a capacitance and a charge relaxation resistance is elusive as a result of unconventional scaling laws.

Another important assumption in our work is that the Friedel sum rule is satisfied. This seems to be the case for the two models we investigated, but it is certainly not general, even for a Fermi liquid fixed point. However, the fact that dissipation comes from the time-dependence in the phase shift felt by lead electrons does not rely on the Friedel sum rule and should apply to more general models such as double-dot geometries. Also we only considered the case of zero temperature or temperatures much smaller than the charging energy. At higher temperatures, inelastic modes are excited and the analysis presented here is not applicable.

In order to put the Fermi liquid picture on firm grounds, we calculated, based on a renormalization group analysis, the low-energy theory for two representative models describing the quantum RC circuit: the Anderson and the Coulomb blockade models. In addition to providing an alternative demonstration of the mapping from the Anderson to the Kondo model, we find that the phenomenological low-energy theory proposed in this paper is recovered perturbatively for the two models. The Friedel sum rule was also checked explicitly.

We conclude with a technical remark regarding Ref. 53 where the case of a tunnel junction (infinite N) was considered. The definition of the charge relaxation resistance R_q involves formally the limit of vanishing frequency $\omega \to 0$. At finite temperature, this limit does not commute with an expansion in the tunneling g or Γ as emphasized in Ref. 53 (see also Ref. 103). At zero temperature, however, the two limits commute[104] and the perturbative expansion of Sec. III becomes justified. Moreover, at finite by small temperatures, a large frequency $\hbar\omega \gg k_B T$ is sufficient to suppress the singular term $\propto 1/\omega$ and the results of Sec. III are still valid.

ACKNOWLEDGMENTS

We thank K. Le Hur and L. Glazman for stimulating discussions.

APPENDIX A: CALCULATION OF THE VERTEX $\mathcal{V}^a$

Once we consider that

$$(\mathbf{S}_{\beta\tau}\cdot\mathbf{s}_{\alpha\sigma})(\mathbf{S}_{\tau'\beta}\cdot\mathbf{s}_{\sigma'\alpha}) = -\tfrac{1}{2}\mathbf{S}_{\tau'\tau}\cdot s_{\sigma'\sigma} + \tfrac{3}{16}\delta_{\tau\tau'}\delta_{\sigma\sigma'}, \quad \text{(A1)}$$

it is possible to determine which term will contribute to the exchange and to the potential scattering part of the vertex $\mathcal{V}^a = \mathbf{S}\cdot\mathbf{s}\mathcal{V}^a_J + \mathcal{V}^a_K$, where

$$\mathcal{V}^a_J = 4\frac{t^4}{\beta}\sum_{k,i\omega_n} F(i\omega_n)G_k(i\omega_\Lambda + i\omega - i\omega_n)\big[F_2^2(i\omega_\Lambda + i\omega) + F_2(i\omega_\Lambda + i\omega)F_0(i\omega_n - i\omega)\big], \quad \text{(A2a)}$$

$$\mathcal{V}^a_K = -\frac{t^4}{\beta}\sum_{k,i\omega_n} F(i\omega_n)G_k(i\omega_\Lambda + i\omega - i\omega_n)\big[F_0^2(i\omega_n - i\omega) + F_2^2(i\omega_\Lambda + i\omega) + F_0(i\omega_n - i\omega)F_2(i\omega_\Lambda + i\omega)\big]. \quad \text{(A2b)}$$

We detail the calculation of the Matsubara sums only for the following example:

$$\begin{aligned}\frac{1}{\beta}\sum_{k,i\omega_n} F(i\omega_n)G_k(i\omega_\Lambda + i\omega - i\omega_n)F_0^2(i\omega_n - i\omega) &= \nu_0\int_{-D_0}^{D_0} d\varepsilon\left[\frac{f(\lambda)}{(i\omega_\Lambda + i\omega - \lambda - \varepsilon)(\varepsilon_d - i\omega)^2}\right.\\ &\quad - \frac{f(i\omega_\Lambda + i\omega - \varepsilon)}{(i\omega_\Lambda + \varepsilon_d - \lambda - \varepsilon)^2(i\omega_\Lambda + i\omega - \varepsilon - \lambda)}\\ &\quad \left. + \frac{d}{dz}\frac{f(z)}{(z-\lambda)(i\omega_\Lambda + i\omega - z - \varepsilon)}\bigg|_{z=i\omega+\lambda-\varepsilon_d}\right]. \quad \text{(A3)}\end{aligned}$$

Notice $f(i\omega_\Lambda + i\omega - \varepsilon) = f(-\varepsilon)$. The analytical continuations of Eq. (52) can now be performed and the first deviation from λ of $\tilde{\varepsilon}_d$ in Eq. (57) can be neglected to this order. The denominators do not depend on λ anymore and, as required by the projection technique, the $\lambda \to \infty$ limit can be taken. All the contributions of the poles that were proportional to λ disappear and the only remaining integral is

$$\nu_0\int_0^{D_0}\frac{d\varepsilon}{(\varepsilon+\Lambda)(\varepsilon_d-\varepsilon)^2} = \frac{\nu_0}{\varepsilon_d^2}\left(\ln\frac{-\varepsilon_d}{D_0} - \ln\frac{\Lambda}{D_0} - 1\right).$$

It is also possible to take the infinite bandwidth limit $D_0 \to \infty$ in this expression, but it is convenient to keep a finite cutoff for the moment. The same kind of calculations gives analog results for the remaining sums:

$$\begin{aligned}\frac{1}{\beta}\sum_{k,i\omega_n} F(i\omega_n)G_k(i\omega_\Lambda + i\omega - i\omega_n)F_0(i\omega_n - i\omega)F_2(i\omega_\Lambda + i\omega) &= \frac{\nu_0}{\varepsilon_d(\varepsilon_d + U)}\left(\ln\frac{\Lambda}{D_0} - \ln\frac{-\varepsilon_d}{D_0}\right), \quad \text{(A4)}\end{aligned}$$

$$\frac{1}{\beta}\sum_{k,i\omega_n} F(i\omega_n)G_k(i\omega_\Lambda + i\omega_i\omega_n)F_2^2(i\omega_\Lambda + i\omega) = -\frac{\nu_0}{(\varepsilon_d+U)^2}\ln\frac{\Lambda}{D_0}. \quad \text{(A5)}$$

These last expressions allow us to obtain Eq. (63).

APPENDIX B: INTEGRATION OF THE HIGH-ENERGY MODES IN THE COULOMB BLOCKADE MODEL

The action Eq. (78) being quadratic in the high-energy modes $b_{\pm 2}$, their integration is straightforward and brings separate terms to the effective action:

$$b_2 : t^2 \sum_{kk'll'\sigma\sigma'} \mathrm{Tr}[c^\dagger_{k\sigma} d_{l\sigma} b_1^\dagger F_2 d^\dagger_{l'\sigma'} c_{k'\sigma'} b_1], \quad \text{(B1a)}$$

$$b_{-2} : t^2 \sum_{kk'll'\sigma\sigma'} \mathrm{Tr}[d^\dagger_{l\sigma} c_{k\sigma} b_{-1}^\dagger F_{-2} c^\dagger_{k'\sigma'} d_{l'\sigma'} b_{-1}]. \quad \text{(B1b)}$$

This action can be written as $S = S_0 + S_1 + S_{-1}$, with

$$S_1 = \mathrm{Tr}\left[-b_1^\dagger \Phi_1^{-1} b_1 + t\sum_{kl\sigma}(c^\dagger_{k\sigma} d_{l\sigma} b_0^\dagger b_1 + d^\dagger_{l\sigma} c_{k\sigma} b_1^\dagger b_0)\right], \quad \text{(B2a)}$$

$$S_{-1} = \mathrm{Tr}\Big[- b_{-1}^\dagger \Phi_{-1}^{-1} b_{-1} + t\sum_{kl\sigma}(c^\dagger_{k\sigma} d_{l\sigma} b_{-1}^\dagger b_0 + d^\dagger_{l\sigma} c_{k\sigma} b_0^\dagger b_{-1})\Big], \quad \text{(B2b)}$$

and the new effective propagators

$$\Phi_1^{-1} = F_1^{-1} - t^2 \sum_{kk'll'\sigma\sigma'} c^\dagger_{k\sigma} d_{l\sigma} F_2 d^\dagger_{l'\sigma'} c_{k'\sigma'}, \quad \text{(B3)}$$

$$\Phi_{-1}^{-1} = F_{-1}^{-1} - t^2 \sum_{kk'll'\sigma\sigma'} d^\dagger_{l\sigma} c_{k\sigma} F_{-2} c^\dagger_{k'\sigma'} d_{l'\sigma'}. \quad \text{(B4)}$$

The integration over the $b_{\pm 1}$ modes is still Gaussian and the effective action without high-energy bosonic modes is finally obtained:

$$S = S_0 + \mathrm{Tr}\Big[-b_0^\dagger F_0^{-1} b_0 + t^2 \sum_{kk'll'\sigma\sigma'} c^\dagger_{k\sigma} d_{l\sigma} b_0^\dagger \Phi_1 d^\dagger_{l'\sigma'} c_{k'\sigma'} b_0 + t^2 \sum_{kk'll'\sigma\sigma'} d^\dagger_{l\sigma} c_{k\sigma} b_0^\dagger \Phi_{-1} c^\dagger_{k'\sigma'} d_{l'\sigma'} b_0\Big]. \quad \text{(B5)}$$

The Φ operators can be expanded perturbatively in t:

$$\Phi_1 = F_1 + t^2 \sum_{kk'll'\sigma\sigma'} F_1 c^\dagger_{k\sigma} d_{l\sigma} F_2 d^\dagger_{l'\sigma'} c_{k'\sigma'} F_1, \quad \text{(B6a)}$$

$$\Phi_{-1} = F_{-1} + t^2 \sum_{kk'll'\sigma\sigma'} F_{-1} d^\dagger_{l\sigma} c_{k\sigma} F_{-2} c^\dagger_{k'\sigma'} d_{l'\sigma'} F_{-1}. \quad \text{(B6b)}$$

This gives the action (78).

APPENDIX C: SUMMATION OF ALL THE CONTRIBUTIONS OF $\mathcal{V}^R$ IN THE COULOMB BLOCKADE MODEL

All the contributions corresponding to the diagrams of Figs. 11 and 12 are listed below (with $\mathcal{C} = N\nu_0^3 t^4$):

$$\begin{aligned}
\mathcal{V}_1 &= -\mathcal{C}\int d\varepsilon_1 d\varepsilon_2 \frac{\varepsilon_1}{(\varepsilon_2+E_1)^2(\varepsilon_1+\varepsilon_2)},\\
\mathcal{V}_2 &= \mathcal{C}\int d\varepsilon_1 d\varepsilon_2 \frac{\varepsilon_1}{(\varepsilon_1+E_1)^2(\varepsilon_1+\varepsilon_2)},\\
\mathcal{V}_3 &= \mathcal{C}\int d\varepsilon_1 d\varepsilon_2 \frac{\varepsilon_1}{(\varepsilon_2+E_{-1})^2(\varepsilon_1+\varepsilon_2)},\\
\mathcal{V}_4 &= -\mathcal{C}\int d\varepsilon_1 d\varepsilon_2 \frac{\varepsilon_1}{(\varepsilon_1+E_{-1})^2(\varepsilon_1+\varepsilon_2)},\\
\mathcal{V}_5 &= -2\mathcal{C}\int d\varepsilon_1 d\varepsilon_2 \frac{\varepsilon_1}{(\varepsilon_1+\varepsilon_2)(\varepsilon_2+E_1)(\varepsilon_1+E_{-1})},\\
\mathcal{V}_6 &= 2\mathcal{C}\int d\varepsilon_1 d\varepsilon_2 \frac{\varepsilon_1}{(\varepsilon_1+\varepsilon_2)(\varepsilon_1+E_1)(\varepsilon_2+E_{-1})},\\
\mathcal{V}_7 &= -\mathcal{C}\int d\varepsilon_1 d\varepsilon_2 \frac{\varepsilon_1}{(\varepsilon_2+E_1)^2(\varepsilon_1+\varepsilon_2+E_2)},\\
\mathcal{V}_8 &= -\mathcal{C}\int d\varepsilon_1 d\varepsilon_2 \frac{\varepsilon_1}{(\varepsilon_1+E_1)^2(\varepsilon_1+\varepsilon_2+E_2)},\\
\mathcal{V}_9 &= -2\mathcal{C}\int d\varepsilon_1 d\varepsilon_2 \frac{\varepsilon_1}{(\varepsilon_2+E_1)(\varepsilon_1+\varepsilon_2+E_2)(\varepsilon_1+E_1)},\\
\mathcal{V}_{10} &= \mathcal{C}\int d\varepsilon_1 d\varepsilon_2 \frac{\varepsilon_1}{(\varepsilon_2+E_{-1})^2(\varepsilon_1+\varepsilon_2+E_{-2})},\\
\mathcal{V}_{11} &= \mathcal{C}\int d\varepsilon_1 d\varepsilon_2 \frac{\varepsilon_1}{(\varepsilon_1+E_{-1})^2(\varepsilon_1+\varepsilon_2+E_{-2})},\\
\mathcal{V}_{12} &= 2\mathcal{C}\int d\varepsilon_1 d\varepsilon_2 \frac{\varepsilon_1}{(\varepsilon_1+E_{-1})(\varepsilon_1+\varepsilon_2+E_{-2})(\varepsilon_2+E_{-1})},
\end{aligned} \quad \text{(C1)}$$

where integrals run over the $\varepsilon_{1,2} > 0$ domain, to which the contributions of Eqs. (86) and (87) must be added. Whereas each term in Eqs. (C1), (86), and (87) suffers from a UV divergence, the summation over all contributions is finite and does not depend on the cutoff procedure. We shall adopt a sharp cutoff at energy D_0 in the following. Moreover, the calculation exhibits a particle-hole symmetry: for example, $\mathcal{V}_3$ can be viewed as the symmetric of $\mathcal{V}_1$, they have opposite sign and E_n exchanged with E_{-n}. The result will then be necessarily of the form $A[\varepsilon_d] - A[-\varepsilon_d]$, which implies that any constant independent of ε_d will be ignored during calculations. The dilogarithm function appears

$$Li_2(z) = \int_z^0 dt \frac{\ln(1-t)}{t}, \quad \text{(C2)}$$

and the following equalities will be exploited:

$$Li_2(x) + Li_2(1-x) = \frac{\pi^2}{6} - \ln x \ln(1-x), \quad \text{(C3a)}$$

$$Li_2(x) + Li_2\left(\frac{1}{x}\right) = \frac{\pi^2}{3} - \frac{1}{2}\ln^2 x - i\pi \ln x, (x \geqslant 1). \quad \text{(C3b)}$$

As an intermediate step, we find (we omit the $N\nu_0^3 t^4$ factor)

$$\begin{aligned}
\mathcal{V}_1+\mathcal{V}_2 &= -\frac{D_0}{E_1} - 2\ln E_1 \ln D_0 + \ln^2 D_0 \\
&\quad - 2\ln D_0 + \ln^2 E_1 + 2\ln E_1, \\
\mathcal{V}_7+\mathcal{V}_8 &= -\frac{D_0}{E_1} + \frac{E_2}{E_1}\ln D_0 \\
&\quad + \frac{1}{E_1(E_2-E_1)}\left(E_1E_2\ln E_1 - E_2^2\ln E_2\right), \\
\mathcal{V}_5+\mathcal{V}_6+\mathcal{V}'' &= -\frac{\varepsilon_d}{E_c}\pi^2 - \frac{\varepsilon_d}{E_c}\ln^2\frac{E_1}{E_{-1}} + 2\ln\frac{E_1}{E_{-1}}, \\
\mathcal{V}_9 &= 2\ln E_1\ln D_0 - \ln^2 D_0 + \frac{E_1}{E_c}\ln^2 E_1 \\
&\quad - \frac{E_1}{E_c}\frac{\pi^2}{2} + \frac{E_2}{E_c}\frac{\pi^2}{6} + \frac{E_2}{E_c}Li_2\left(\frac{E_2-E_1}{E_2}\right) \\
&\quad + \frac{E_2}{2E_c}\ln^2 E_2 - \frac{E_2}{E_c}\ln E_1\ln E_2,
\end{aligned}$$

with the contribution of Eq. (86):

$$\mathcal{V}' = \nu_0 t^2 \ln\frac{E_1}{E_{-1}} + N\nu_0^3 t^4(\mathcal{V}'_a + \mathcal{V}'_b), \tag{C4}$$

$$\begin{aligned}
\mathcal{V}'_a &= \int d\varepsilon_1 d\varepsilon_2 \frac{1}{(\varepsilon_2+E_1)}\left[\frac{\varepsilon_1}{(\varepsilon_1+E_1)} + \frac{\varepsilon_1}{(\varepsilon_1+E_{-1})}\right] \\
&= \frac{2D_0}{E_1} - \ln D_0 - \frac{E_{-1}}{E_1}\ln D_0 + \ln E_1 + \frac{E_{-1}}{E_1}\ln E_{-1},
\end{aligned} \tag{C5}$$

where $\mathcal{V}'_b$ is obtained from $\mathcal{V}'_a$ by particle-hole symmetry. It can be checked explicitly that the terms depending on the cutoff D_0 in the above expressions cancel out when the summation over all contributions is carried out. One is left with

$$\begin{aligned}
\mathcal{V}_1+\mathcal{V}_2 &= \ln^2 E_1 + 2\ln E_1, \\
\mathcal{V}_7+\mathcal{V}_8 &= \frac{1}{E_1(E_2-E_1)}\left(E_1E_2\ln E_1 - E_2^2\ln E_2\right), \\
\mathcal{V}'_a &= \ln E_1 + \frac{E_{-1}}{E_1}\ln E_{-1}, \\
\mathcal{V}_5+\mathcal{V}_6+\mathcal{V}'' &= -\frac{\varepsilon_d}{E_c}\pi^2 - \frac{\varepsilon_d}{E_c}\ln^2\frac{E_1}{E_{-1}} + 2\ln\frac{E_1}{E_{-1}}, \\
\mathcal{V}_9 &= \frac{E_1}{E_c}\ln^2 E_1 - \frac{E_1}{E_c}\frac{\pi^2}{2} + \frac{E_2}{E_c}\frac{\pi^2}{6} + \frac{E_2}{2E_c}\ln^2 E_2 \\
&\quad + \frac{E_2}{E_c}Li_2\left(\frac{E_2-E_1}{E_2}\right) - \frac{E_2}{E_c}\ln E_1\ln E_2.
\end{aligned}$$

Adding the particle-hole symmetric terms, one finally arrives at Eq. (90).

[1] H. Pothier, P. Lafarge, C. Urbina, D. Esteve, and M. Devoret, Europhys. Lett. **17**, 249 (1992).
[2] M. Büttiker, H. Thomas, and A. Prêtre, Z. Phys. B: Condens. Matter **94**, 133 (1994).
[3] P. W. Brouwer, Phys. Rev. B **58**, R10135 (1998).
[4] I. L. Aleiner and A. V. Andreev, Phys. Rev. Lett. **81**, 1286 (1998).
[5] P. J. Leek, M. R. Buitelaar, V. I. Talyanskii, C. G. Smith, D. Anderson, G. A. C. Jones, J. Wei, and D. H. Cobden, Phys. Rev. Lett. **95**, 256802 (2005).
[6] J. Splettstoesser, M. Governale, J. König, and R. Fazio, Phys. Rev. B **74**, 085305 (2006).
[7] R. Schleser, E. Ruh, T. Ihn, K. Ensslin, D. C. Driscoll, and A. C. Gossard, Appl. Phys. Lett. **85**, 2005 (2004).
[8] L. M. K. Vandersypen, J. M. Elzerman, R. N. Schouten, L. H. W. van Beveren, R. Hanson, and L. P. Kouwenhoven, Appl. Phys. Lett. **85**, 4394 (2004).
[9] L. P. Kouwenhoven, S. Jauhar, J. Orenstein, P. L. McEuen, Y. Nagamune, J. Motohisa, and H. Sakaki, Phys. Rev. Lett. **73**, 3443 (1994).
[10] A. Kogan, S. Amasha, and M. A. Kastner, Science **304**, 1293 (2004).
[11] R. J. Schoelkopf, P. Wahlgren, A. A. Kozhevnikov, P. Delsing, and D. E. Prober, Science **280**, 1238 (1998).
[12] R. Aguado and L. P. Kouwenhoven, Phys. Rev. Lett. **84**, 1986 (2000).
[13] E. Onac, F. Balestro, L. H. W. van Beveren, U. Hartmann, Y. V. Nazarov, and L. P. Kouwenhoven, Phys. Rev. Lett. **96**, 176601 (2006).
[14] S. Gustavsson, M. Studer, R. Leturcq, T. Ihn, K. Ensslin, D. C. Driscoll, and A. C. Gossard, Phys. Rev. Lett. **99**, 206804 (2007).
[15] R. Deblock, E. Onac, L. Gurevich, and L. P. Kouwenhoven, Science **301**, 203 (2003).
[16] P.-M. Billangeon, F. Pierre, H. Bouchiat, and R. Deblock, Phys. Rev. Lett. **96**, 136804 (2006).
[17] J. Basset, H. Bouchiat, and R. Deblock, Phys. Rev. Lett. **105**, 166801 (2010).
[18] W. Xue, Z. Ji, F. Pan, J. Stettenheim, M. Blencowe, and A. Rimberg, Nat. Phys. **5**, 660 (2009).
[19] E. Zakka-Bajjani, J. Ségala, F. Portier, P. Roche, D. C. Glattli, A. Cavanna, and Y. Jin, Phys. Rev. Lett. **99**, 236803 (2007).
[20] J. Gabelli and B. Reulet, Phys. Rev. Lett. **100**, 026601 (2008).
[21] E. Zakka-Bajjani, J. Dufouleur, N. Coulombel, P. Roche, D. C. Glattli, and F. Portier, Phys. Rev. Lett. **104**, 206802 (2010).
[22] J. Gabelli, G. Fève, J.-M. Berroir, B. Plaçais, A. Cavanna, B. Etienne, Y. Jin, and D. C. Glattli, Science **313**, 499 (2006).
[23] G. Fève, A. Mahé, J.-M. Berroir, T. Kontos, B. Plaçais, D. C. Glattli, A. Cavanna, B. Etienne, and Y. Jin, Science **316**, 1169 (2007).
[24] A. Mahé, F. D. Parmentier, E. Bocquillon, J.-M. Berroir, D. C. Glattli, T. Kontos, B. Plaçais, G. Fève, A. Cavanna, and Y. Jin, Phys. Rev. B **82**, 201309 (2010).
[25] F. D. Parmentier, E. Bocquillon, J.-M. Berroir, D. C. Glattli, B. Plaçais, G. Fève, M. Albert, C. Flindt, and M. Büttiker, Phys. Rev. B **85**, 165438 (2012).
[26] M. R. Delbecq, V. Schmitt, F. D. Parmentier, N. Roch, J. J. Viennot, G. Fève, B. Huard, C. Mora, A. Cottet, and T. Kontos, Phys. Rev. Lett. **107**, 256804 (2011).
[27] T. Frey, P. J. Leek, M. Beck, A. Blais, T. Ihn, K. Ensslin, and A. Wallraff, Phys. Rev. Lett. **108**, 046807 (2012).

[28] F. Persson, C. M. Wilson, M. Sandberg, G. Johansson, and P. Delsing, Nano Lett. **10**, 953 (2010).
[29] C. Ciccarelli and A. J. Ferguson, New J. Phys. **13**, 093015 (2011).
[30] S. J. Chorley, J. Wabnig, Z. V. Penfold-Fitch, K. D. Petersson, J. Frake, C. G. Smith, and M. R. Buitelaar, Phys. Rev. Lett. **108**, 036802 (2012).
[31] A. Cottet, C. Mora, and T. Kontos, Phys. Rev. B **83**, 121311 (2011).
[32] M. Büttiker, A. Prêtre, and H. Thomas, Phys. Rev. Lett. **70**, 4114 (1993).
[33] M. Büttiker, H. Thomas, and A. Prêtre, Phys. Lett. A **180**, 364 (1993).
[34] A. Prêtre, H. Thomas, and M. Büttiker, Phys. Rev. B **54**, 8130 (1996).
[35] V. A. Gopar, P. A. Mello, and M. Büttiker, Phys. Rev. Lett. **77**, 3005 (1996).
[36] P. W. Brouwer, K. M. Frahm, and C. W. J. Beenakker, Phys. Rev. Lett. **78**, 4737 (1997).
[37] P. W. Brouwer and M. Büttiker, Europhys. Lett. **37**, 441 (1997).
[38] M. H. Pedersen, S. A. van Langen, and M. Büttiker, Phys. Rev. B **57**, 1838 (1998).
[39] M. Büttiker, J. Korean Phys. Soc. **34**, S121 (1999).
[40] M. Büttiker and M. L. Polianski, J. Phys. A **38**, 10559 (2005).
[41] P. W. Brouwer, A. Lamacraft, and K. Flensberg, Phys. Rev. B **72**, 075316 (2005).
[42] J. Wang, B. Wang, and H. Guo, Phys. Rev. B **75**, 155336 (2007).
[43] Y. M. Blanter, F. W. J. Hekking, and M. Büttiker, Phys. Rev. Lett. **81**, 1925 (1998).
[44] K. Pham, Eur. Phys. J. B **36**, 607 (2003).
[45] S. E. Nigg and M. Büttiker, Phys. Rev. B **77**, 085312 (2008).
[46] M. Büttiker and S. E. Nigg, Eur. Phys. J. Special Topics **172**, 247 (2009).
[47] S. E. Nigg, R. López, and M. Büttiker, Phys. Rev. Lett. **97**, 206804 (2006).
[48] M. Büttiker and S. E. Nigg, Nanotechnology **18**, 044029 (2007).
[49] Z. Ringel, Y. Imry, and O. Entin-Wohlman, Phys. Rev. B **78**, 165304 (2008).
[50] J. Splettstoesser, M. Governale, J. König, and M. Büttiker, Phys. Rev. B **81**, 165318 (2010).
[51] S. E. Nigg and M. Büttiker, Phys. Rev. Lett. **102**, 236801 (2009).
[52] I. Garate and K. Le Hur, Phys. Rev. B **85**, 195465 (2012).
[53] Y. I. Rodionov, I. S. Burmistrov, and A. S. Ioselevich, Phys. Rev. B **80**, 035332 (2009).
[54] C. Petitjean, D. Waltner, J. Kuipers, I. Adagideli, and K. Richter, Phys. Rev. B **80**, 115310 (2009).
[55] Y. Etzioni, B. Horovitz, and P. Le Doussal, Phys. Rev. Lett. **106**, 166803 (2011).
[56] M. Moskalets, P. Samuelsson, and M. Büttiker, Phys. Rev. Lett. **100**, 086601 (2008).
[57] J. Keeling, A. V. Shytov, and L. S. Levitov, Phys. Rev. Lett. **101**, 196404 (2008).
[58] M. Albert, C. Flindt, and M. Büttiker, Phys. Rev. B **82**, 041407 (2010).
[59] M. Albert, C. Flindt, and M. Büttiker, Phys. Rev. Lett. **107**, 086805 (2011).
[60] S. Andergassen, M. Pletyukhov, D. Schuricht, H. Schoeller, and L. Borda, Phys. Rev. B **83**, 205103 (2011).
[61] O. Kashuba, H. Schoeller, and J. Splettstoesser, EPL **98**, 57003 (2012).
[62] L. Debora Contreras-Pulido, J. Splettstoesser, M. Governale, J. König, and M. Büttiker, Phys. Rev. B **85**, 075301 (2012).
[63] C. Mora and K. Le Hur, Nat. Phys. **6**, 697 (2010).
[64] Y. Hamamoto, T. Jonckheere, T. Kato, and T. Martin, Phys. Rev. B **81**, 153305 (2010).
[65] L. Glazman and K. A. Matveev, Zh. Eksp. Teor. Fiz. **98**, 1834 (1990) [Sov. Phys. JETP **71**, 1031 (1990)].
[66] K. A. Matveev, Zh. Eksp. Teor. Fiz. **99**, 1598 (1991) [Sov. Phys. JETP **72**, 892 (1991)].
[67] A. Furusaki and K. A. Matveev, Phys. Rev. Lett. **88**, 226404 (2002).
[68] A. C. Hewson, *The Kondo Problem to Heavy Fermions* (Cambridge University Press, Cambridge, 1993).
[69] H. Shiba, Prog. Theor. Phys. **54**, 967 (1975).
[70] M. Lee, R. López, M.-S. Choi, T. Jonckheere, and T. Martin, Phys. Rev. B **83**, 201304 (2011).
[71] M. Filippone, K. Le Hur, and C. Mora, Phys. Rev. Lett. **107**, 176601 (2011).
[72] M. Garst, P. Wölfle, L. Borda, J. von Delft, and L. Glazman, Phys. Rev. B **72**, 205125 (2005).
[73] P. Nozières, J. Low Temp. Phys. **17**, 31 (1974).
[74] I. L. Aleiner and L. I. Glazman, Phys. Rev. B **57**, 9608 (1998).
[75] J. M. Luttinger, Phys. Rev. **121**, 942 (1961).
[76] A. A. Clerk, P. W. Brouwer, and V. Ambegaokar, Phys. Rev. Lett. **87**, 186801 (2001).
[77] D. C. Langreth, Phys. Rev. **150**, 516 (1966).
[78] H. Grabert, Phys. Rev. B **50**, 17364 (1994).
[79] Y. Oreg and D. Goldhaber-Gordon, Phys. Rev. Lett. **90**, 136602 (2003).
[80] M. Pustilnik, L. Borda, L. I. Glazman, and J. von Delft, Phys. Rev. B **69**, 115316 (2004).
[81] R. M. Potok, I. G. Rau, H. Shtrikman, Y. Oreg, and D. Goldhaber-Gordon, Nature (London) **446**, 167 (2007).
[82] N. Kawakami and A. Okiji, Phys. Rev. B **42**, 2383 (1990).
[83] H. R. Krishna-murthy, J. W. Wilkins, and K. G. Wilson, Phys. Rev. B **21**, 1003 (1980); **21**, 1044 (1980).
[84] B. L. Altshuler, Y. Gefen, A. Kamenev, and L. S. Levitov, Phys. Rev. Lett. **78**, 2803 (1997).
[85] F. D. M. Haldane, Phys. Rev. Lett. **40**, 416 (1978).
[86] D. Cragg and P. Lloyd, J. Phys. C **11**, L597 (1978).
[87] P. Lloyd and D. M. Cragg, J. Phys. C **12**, 3289 (1979).
[88] D. M. Cragg and P. Lloyd, J. Phys. C **12**, 3301 (1979).
[89] B. Horvatić and V. Zlatić, J. Phys. France **46**, 1459 (1985).
[90] F. D. M. Haldane, J. Phys. C **11**, 5015 (1978).
[91] E. Lebanon, A. Schiller, and F. B. Anders, Phys. Rev. B **68**, 041311 (2003).
[92] H. Grabert, Physica B **194**, 1011 (1994).
[93] J. R. Schrieffer and P. A. Wolff, Phys. Rev. **149**, 491 (1966).
[94] S. E. Barnes, J. Phys. F **6**, 1375 (1976).
[95] A. A. Abrikosov and A. A. Migdal, J. Low Temp. Phys. **3**, 519 (1970).
[96] M. Fowler and A. Zawadowski, Solid State Commun. **9**, 471 (1971).
[97] M. Fowler, Phys. Rev. B **6**, 3422 (1972).
[98] J. Solyom, J. Phys. F **4**, 2269 (1974).
[99] A. A. Abrikosov, Physics **2**, 5 (1965) .
[100] N. Andrei, K. Furuya, and J. H. Lowenstein, Rev. Mod. Phys. **55**, 331 (1983).
[101] N. Andrei and J. H. Lowenstein, Phys. Rev. Lett. **46**, 356 (1981).
[102] A. M. Tsvelick and P. B. Wiegmann, Adv. Phys. **32**, 453 (1983).
[103] W. Götze and P. Wölfle, J. Low Temp. Phys. **5**, 575 (1971).
[104] This can be seen, for example, by noting that the singular term $\propto 1/\omega$ given by Eq. (75) in Ref. 53 vanishes at zero temperature.